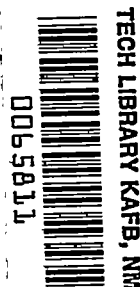# NATIONAL ADVISORY COMMITTEE FOR AERONAUTICS

TECHNICAL NOTE 2858

SUPERSONIC WAVE DRAG OF NONLIFTING DELTA WINGS WITH

LINEARLY VARYING THICKNESS RATIO

By Arthur Henderson, Jr.

Langley Aeronautical Laboratory
Langley Field, Va.

NACA

Washington

December 1952

NATIONAL ADVISORY COMMITTEE FOR AERONAUTICS

TECHNICAL NOTE 2858

SUPERSONIC WAVE DRAG OF NONLIFTING DELTA WINGS WITH

LINEARLY VARYING THICKNESS RATIO

By Arthur Henderson, Jr.

SUMMARY

The supersonic wave drag of a nonlifting, symmetrical, double-wedge-profile, delta wing the thickness ratio of which varies linearly in the spanwise direction is calculated by means of linear theory.

In general it is found that a delta wing with linearly varying thickness ratio can have less wave drag than a constant-thickness-ratio delta wing of the same plan form when both wings have either the same projected frontal area or the same internal volume. The thickness distributions for minimum drag and the corresponding values of the ratio of the drag of a linearly varying thickness-ratio wing to a constant-thickness-ratio wing are found.

INTRODUCTION

In reference 1, Puckett has found the supersonic wave drag of a nonlifting, symmetrical, double-wedge-profile, delta wing with constant thickness ratio. It is shown that the drag coefficient for the delta wing may be reduced below the two-dimensional value only for the case in which both the leading edge and the ridge line are subsonic, the maximum reduction for a given Mach number and semiapex angle being a function of the position of the ridge line.

In the present paper the additional effect on the drag of varying the thickness ratio in the spanwise direction is determined with the assumption that the thickness ratio varies linearly in the spanwise direction, which means that, when the wing is viewed from behind, the line of maximum thickness has a parabolic shape. The source-distribution method developed in reference 1 is used to represent the variable-thickness-ratio wings.

It is shown that the deviation of the maximum-thickness line from a straight line can be represented by a nondimensional parameter. Charts are presented from which, if this parameter is known, the drag of a variable-thickness-ratio delta wing can be found. Also shown is the fact

that a delta wing with a linearly varying thickness ratio can give less wave drag than a constant-thickness-ratio delta wing when both wings have the same projected frontal area or when both have the same internal volume. The value of the nondimensional maximum-thickness-distribution parameter, for which the ratio of the drag of the variable-thickness-ratio wing to the drag of the constant-thickness-ratio wing is a minimum, is calculated for both criteria.

SYMBOLS

A_f projected frontal area

$a = \beta \epsilon_{RL}$

$B = \dfrac{y}{c_r \epsilon_{LE}} = \dfrac{\beta \left(y/c_r \right)}{b}$

$b = \beta \epsilon_{LE}$

$\beta = \sqrt{M^2 - 1}$

C_D drag coefficient, D/qS

c_r root chord

$c(y)$ local chord

D drag

Δp local static pressure minus free-stream static pressure

ϵ_{LE} tangent of leading-edge semiapex angle

ϵ_{RL} tangent of ridge-line semiapex angle

$\left. \begin{matrix} F_1, F_2, F_3 \\ G_1, G_2, G_3 \\ H_1, H_2, H_3 \end{matrix} \right\}$ functions defined in appendix B

λ slope of airfoil surface in streamwise direction

M   free-stream Mach number

m   dimensional thickness-distribution parameter

$\overline{m}$ nondimensional thickness-distribution parameter,
$$\frac{mc_r\epsilon_{LE}}{\tau} = \frac{mc_r b}{\beta\tau}$$

ξ,η dummy variables for x and y, respectively

P_1 and p_1 pressure-distribution function and $\partial\phi_1/\partial x$ associated
                with basic source distribution when $b < 1$

P_2 and p_2 pressure-distribution function and $\partial\phi_2/\partial x$ associated
                with superimposed source distribution when $a < 1$

$Q_1,\overline{Q}_1$ and $q_1,\overline{q}_1$ pressure-distribution functions and $\partial\phi_1/\partial x$ associated
                with basic source distribution when $b > 1$

$Q_2,\overline{Q}_2$ and $q_2,\overline{q}_2$ pressure-distribution functions and $\partial\phi_2/\partial x$ associated
                with superimposed source distribution when $a > 1$

q   dynamic pressure, $\frac{1}{2}\rho V^2$

$r = \dfrac{\epsilon_{LE}}{\epsilon_{RL}}$

ρ free-stream density

S   plan-form area

t_r root thickness

$t(y)$ local maximum thickness

τ thickness ratio at root, t_r/c_r

$u = \beta\dfrac{y}{x}$

V   free-stream velocity

V_i internal volume

ϕ perturbation velocity potential

w   perturbation velocity in z-direction

x,y,z   Cartesian coordinates (right-handed system), x in
                direction of free-stream velocity

Subscripts:

R   right half of wing

1   basic distribution

2   superimposed distribution

Primes denote constant-thickness-ratio wing.

ANALYSIS

The linearized partial differential equation for the perturbation potential in steady supersonic flow is

$$\beta^2 \frac{\partial^2 \phi}{\partial x^2} - \frac{\partial^2 \phi}{\partial y^2} - \frac{\partial^2 \phi}{\partial z^2} = 0 \qquad (1)$$

When considering a thin symmetrical airfoil at zero angle of attack, for which small disturbances are assumed, the boundary conditions on the surface of the wing may be satisfied, to the first order, in the plane of the wing. Hence

$$\left(\frac{\partial \phi}{\partial z}\right)_{z=0} = w = \lambda V \qquad (2)$$

In reference 1, it is shown that a solution of equation (1) which satisfies condition (2) is that for a source distribution

$$\phi(x,y)_{z=0} = -\frac{1}{\pi} \iint_S \frac{w(\xi,\eta)d\xi \, d\eta}{\sqrt{(x - \xi)^2 - \beta^2(y - \eta)^2}} \qquad (3)$$

where $w(\xi,\eta) = \lambda(\xi,\eta)V$ is proportional to the source strength per unit area and λ is the slope of the airfoil section measured in the streamwise direction. For the wing shown in figure 1, the slope of the surface ahead of the ridge line is equal to the ratio of one-half the local maximum thickness at the ridge line to the part of the local chord ahead of the ridge line; the slope of the rear surface is the negative ratio of one-half of the local maximum thickness at the ridge line to the remainder of the local chord. In the present paper the thickness ratio is assumed to vary linearly with y, or

$$\frac{t(y)}{c(y)} = \frac{t_r}{c_r} + 2my \tag{4}$$

where t_r/c_r is the root thickness ratio, and m is a parameter which determines the shape of the thickness curve in the spanwise direction. Therefore, over the forward part of the wing

$$w(x,y) = \frac{t(y)V}{2(1-r)c(y)} = \frac{V}{(1-r)}\left(\frac{t_r}{2c_r} + my\right) \tag{5a}$$

and over the rear part

$$w(x,y) = -\frac{t(y)V}{2rc(y)} = -\frac{V}{r}\left(\frac{t_r}{2c_r} + my\right) \tag{5b}$$

where $r = \dfrac{\epsilon_{LE}}{\epsilon_{RL}}$ and represents the ridge-line position in percent chord measured from the trailing edge.

In the following analysis $\partial\phi/\partial x$ is evaluated from equation (3) by integrating over the right half of the upper surface of the wing. Inasmuch as the wing shape, and therefore the pressure distribution, is symmetrical with respect to the x-axis, $\partial\phi(x,y)/\partial x$ for the entire upper surface is

$$\frac{\partial \phi(x,y)}{\partial x} = \left[\frac{\partial \phi(x,y)}{\partial x}\right]_R + \left[\frac{\partial \phi(x,-y)}{\partial x}\right]_R \qquad (6)$$

The potential of any point (x,y) is found by integrating over the area of the wing lying within the forward-drawn Mach lines from the point (x,y) in order to obtain the effect on the point of all the sources that can influence it.

The wing of the present paper is represented by a distribution of sources in the plane $z = 0$. This distribution is uniquely determined by the boundary conditions on the wing. Since equation (3) is a solution to a linear partial differential equation, this distribution may be represented by a superposition of source distributions in any manner desired as long as the net result is that prescribed by the boundary conditions. The drag on the wing is then found by computing the drag caused by the pressure field of each source distribution and algebraically adding the results.

In the present analysis two source distributions are used: one, the basic distribution which extends over the entire plan form and follows the law governing the source strengths representing the forward slopes of the wing, and the other, the superimposed distribution which lies in the region bounded by the ridge lines and the trailing edge. The sources in this region have the strengths prescribed by the boundary conditions for this region plus the negative value of the strengths of the first distribution. Thus, when superimposed, the net source distribution for the whole wing is that prescribed by the boundary conditions.

From figure 2(a), the basic source distribution used to represent a delta wing with subsonic leading edge ($\beta \epsilon_{LE} < 1$) can be expressed as

$$\left[\phi_1(x,y)\right]_R = -\frac{V}{\pi(1-r)} \int_0^y \int_{\eta/\epsilon_{LE}}^{x-\beta(y-\eta)} \frac{\left(\frac{t_r}{2c_r} + m\eta\right) d\xi \, d\eta}{\sqrt{(x-\xi)^2 - \beta^2(y-\eta)^2}} -$$

$$\frac{V}{\pi(1-r)} \int_y^{\frac{\epsilon_{LE}(x+\beta y)}{1+\beta\epsilon_{LE}}} \int_{\eta/\epsilon_{LE}}^{x+\beta(y-\eta)} \frac{\left(\frac{t_r}{2c_r} + m\eta\right) d\xi \, d\eta}{\sqrt{(x-\xi)^2 - \beta^2(y-\eta)^2}}$$

$$(7)$$

and the superimposed source distribution when the ridge line is sub-
sonic ($\beta\epsilon_{RL} < 1$), as

$$
\left[\phi_2(x,y)\right]_R = \frac{V}{\pi r(1-r)} \int_0^y \int_{\eta/\epsilon_{RL}}^{x-\beta(y-\eta)} \frac{\left(\frac{t_r}{2c_r} + m\eta\right)d\xi\ d\eta}{\sqrt{(x-\xi)^2 - \beta^2(y-\eta)^2}} +
$$

$$
\frac{V}{\pi r(1-r)} \int_y^{\frac{\epsilon_{RL}(x+\beta y)}{1+\beta\epsilon_{RL}}} \int_{\eta/\epsilon_{RL}}^{x+\beta(y-\eta)} \frac{\left(\frac{t_r}{2c_r} + m\eta\right)d\xi\ d\eta}{\sqrt{(x-\xi)^2 - \beta^2(y-\eta)^2}}
$$

$$\tag{8}$$

By the use of equations (6) and (7), a solution for the basic distribu-
tion is obtained:

$$
\frac{\partial\phi_1}{\partial x} = -\frac{2V\left(\frac{t_r}{2c_r}\right)b}{\beta\pi(1-r)\sqrt{1-b^2}} \tanh^{-1}\frac{\sqrt{1-b^2}}{\sqrt{1-u^2}} -
$$

$$
\frac{2Vmb^2x}{\beta^2\pi(1-r)(1-b^2)^{3/2}} \tanh^{-1}\frac{\sqrt{1-b^2}}{\sqrt{1-u^2}} +
$$

$$
\frac{2Vmb^3ux}{\beta^2\pi(1-r)(1-b^2)^{3/2}} \tanh^{-1}\frac{u\sqrt{1-b^2}}{b\sqrt{1-u^2}} +
$$

$$
\frac{2Vmb^2x}{\beta^2\pi(1-r)(1-b^2)} \sqrt{1-u^2}
$$

$$
= p_1(m,r,x,u,b)
$$

$$\tag{9}$$

where $u = \beta\frac{y}{x}$, $b = \beta\epsilon_{LE}$, and $a = \beta\epsilon_{RL}$. Equation (9) is obtained in appendix A. Similarly, equations (6) and (8) produce the solution for the superimposed distribution:

$$\frac{\partial\phi_2}{\partial x} = p_2 = -\frac{1}{r} p_1(m,r,x;u,a) \tag{10}$$

The expression for the potential of the basic source distribution used to represent a delta wing the leading edge of which is supersonic ($\beta\epsilon_{LE} > 1$) is similar to equation (7); however, since in this case the Mach lines from the apex lie on the wing, there are two regions of integration (fig. 2(b)). One is the region interior to the Mach lines where the right and left halves of the wing are interdependent and ϕ_{1_R} is exactly equation (7). The integral is evaluated differently, however, since $\beta\epsilon_{LE} > 1$. The other is the region that lies between the Mach lines and the leading edge where the flow is two-dimensional. Here the right and left regions are independent of each other, and the expression for the potential on one side also gives the potential for the other.

For the region of the wing exterior to the Mach lines,

$$\phi_1 = -\frac{V}{\pi(1-r)}\int_{\frac{\epsilon_{LE}(x-\beta y)}{1-\beta\epsilon_{LE}}}^{y}\int_{\frac{\eta}{\epsilon_{LE}}}^{x-\beta(y-\eta)}\frac{\left(\frac{t_r}{2c_r}+m\eta\right)d\xi\,d\eta}{\sqrt{(x-\xi)^2-\beta^2(y-\eta)^2}} -$$

$$\frac{V}{\pi(1-r)}\int_{y}^{\frac{\epsilon_{LE}(x+\beta y)}{1+\beta\epsilon_{LE}}}\int_{\eta/\epsilon_{LE}}^{x+\beta(y-\eta)}\frac{\left(\frac{t_r}{2c_r}+m\eta\right)d\xi\,d\eta}{\sqrt{(x-\xi)^2-\beta^2(y-\eta)^2}}$$

$$\tag{11}$$

which, with equation (7), yields for a supersonic-leading-edge delta wing, when $0 \leqq u \leqq 1$

$$\frac{\partial \phi_1}{\partial x} = -\frac{2V\left(\frac{t_r}{2c_r}\right)b}{\beta\pi(1-r)\sqrt{b^2-1}} \tan^{-1}\frac{\sqrt{b^2-1}}{\sqrt{1-u^2}} +$$

$$\frac{2Vmb^2x}{\beta^2\pi(1-r)(b^2-1)^{3/2}} \tan^{-1}\frac{\sqrt{b^2-1}}{\sqrt{1-u^2}} -$$

$$\frac{2Vmb^3ux}{\beta^2\pi(1-r)(b^2-1)^{3/2}} \tan^{-1}\frac{u\sqrt{b^2-1}}{b\sqrt{1-u^2}} -$$

$$\frac{2Vmb^2x}{\beta^2\pi(1-r)(b^2-1)}\sqrt{1-u^2}$$

$$= q_1(m,r,x,u,b) \tag{12a}$$

and, when $1 \leqq u \leqq b$

$$\frac{\partial \phi_1}{\partial x} = -\frac{V\left(\frac{t_r}{2c_r}\right)b}{\beta(1-r)\sqrt{b^2-1}} - \frac{Vmb^3ux}{\beta^2(1-r)(b^2-1)^{3/2}} + \frac{Vmb^2x}{\beta^2(1-r)(b^2-1)^{3/2}}$$

$$= \bar{q}_1(m,r,x,u,b) \tag{12b}$$

The corresponding functions for the superimposed source distribution when the ridge line is supersonic are for $0 \leqq u \leqq 1$

$$\frac{\partial \phi_2}{\partial x} = q_2 = -\frac{1}{r} q_1(m,r,x,u,a) \tag{13a}$$

and, for $1 \leqq u \leqq a$,

$$\frac{\partial \phi_2}{\partial x} = \bar{q}_2 = -\frac{1}{r} \bar{q}_1(m,r,x,u,a) \tag{13b}$$

The parameter m in the preceding equations has the dimensions of $(\text{length})^{-1}$. It will be useful to examine the curves of thickness plotted against spanwise distance that can be produced by a variation of m (fig. 3) with the purpose of forming a new dimensionless parameter which includes m. From equation (4), a nondimensional form of the thickness curve is

$$\frac{t(y)}{t_r} = c(y)\left(\frac{1}{c_r} + \frac{2my}{t_r}\right) \tag{14}$$

and since, from figure 1, $c(y) = c_r - \dfrac{y}{\epsilon_{LE}}$

$$\frac{t(y)}{t_r} = 1 + \left(\frac{2m}{\tau} - \frac{1}{c_r \epsilon_{LE}}\right)y - \frac{2m}{t_r \epsilon_{LE}} y^2$$

$$= 1 + \left(\frac{2mc_r \epsilon_{LE}}{\tau} - 1\right)\frac{y}{c_r \epsilon_{LE}} - \frac{2mc_r \epsilon_{LE}}{\tau}\left(\frac{y}{c_r \epsilon_{LE}}\right)^2$$

$$= 1 + \left(\frac{2mc_r b}{\beta\tau} - 1\right)\frac{\beta\left(y/c_r\right)}{b} - \frac{2mc_r b}{\beta\tau}\left[\frac{\beta\left(y/c_r\right)}{b}\right]^2 \tag{15a}$$

where

$$0 \leqq \frac{\beta\left(y/c_r\right)}{b} \leqq 1$$

The nondimensional thickness-distribution parameter is, therefore, taken to be $mc_r b/\beta\tau$ which is hereinafter denoted by $\bar{m}$. Equation (15a) may be rewritten as follows:

$$\frac{t(y)}{t_r} = 1 + (2\overline{m} - 1)B - 2\overline{m}B^2 \tag{15b}$$

where

$$B = \frac{\beta\left(y/c_r\right)}{b}$$

Equation (15b) is a quadratic in B and represents a parabola. If the type of curve for equation (15b) is known, one absolute limit on $\overline{m}$ can be established. This limit can be determined since, at the wing tip the slope of the thickness curve cannot be less than zero. For this case, $\overline{m} = -\frac{1}{2}$. When the slope of the thickness curve is zero at the root, $\overline{m} = \frac{1}{2}$; however, this value is not necessarily an upper limit. Curves of thickness distribution for different values of $\overline{m}$ are shown in figure 3.

PRESSURE DISTRIBUTION

To the first order, the pressure on the surface of the wing is given by

$$\frac{\Delta p}{q} = -\frac{2}{V}\left(\frac{\partial\phi}{\partial x}\right)_{z=0} \tag{16}$$

Introducing the parameter $\overline{m}$ into equations (9), (10), (12a), (12b), (13a), and (13b) and using equation (16) gives the pressure equations in the following forms:

For the basic subsonic-leading-edge delta wing

$$\frac{\Delta p}{q} = \frac{2\tau b}{\beta\pi(1-r)\sqrt{1-b^2}}\tanh^{-1}\frac{\sqrt{1-b^2}}{\sqrt{1-u^2}} +$$

$$\frac{4\overline{m}b\left(\frac{x}{c_r}\right)\tau}{\beta\pi(1-r)(1-b^2)}\left(\frac{1}{\sqrt{1-b^2}}\tanh^{-1}\frac{\sqrt{1-b^2}}{\sqrt{1-u^2}} - \right.$$

$$\frac{bu}{\sqrt{1-b^2}}\tanh^{-1}\frac{u\sqrt{1-b^2}}{b\sqrt{1-u^2}} - \sqrt{1-u^2}\left.\right)$$

$$= P\left(\overline{m}, r, \frac{x}{c_r}, u, b\right) = P_1 \qquad\qquad (0 \leqq u < b) \tag{17}$$

For the superimposed subsonic-leading-edge delta wing

$$\frac{\Delta p}{q} = -\frac{1}{r} \, P\!\left(\overline{m}, r, \frac{x}{c_r}, u, a\right) = -\frac{1}{r} \, P_2 \qquad (0 \leqq u < a) \qquad\qquad (18)$$

For the basic supersonic-leading-edge delta wing

$$\frac{\Delta p}{q} = \frac{2\tau b}{\beta \pi (1 - r) \sqrt{b^2 - 1}} \tan^{-1} \frac{\sqrt{b^2 - 1}}{\sqrt{1 - u^2}} -$$

$$\frac{4\overline{m}b\!\left(\dfrac{x}{c_r}\right)\tau}{\beta \pi (1 - r)(b^2 - 1)} \!\left(\frac{1}{\sqrt{b^2 - 1}} \tan^{-1} \frac{\sqrt{b^2 - 1}}{\sqrt{1 - u^2}} -\right.$$

$$\left.\frac{bu}{\sqrt{b^2 - 1}} \tan^{-1} \frac{u\sqrt{b^2 - 1}}{b\sqrt{1 - u^2}} - \sqrt{1 - u^2}\right)$$

$$= Q\!\left(\overline{m}, r, \frac{x}{c_r}, u, b\right) = Q_1 \qquad\qquad (0 \leqq u \leqq 1) \qquad (19a)$$

$$\frac{\Delta p}{q} = \frac{\tau b}{\beta (1 - r)\sqrt{b^2 - 1}} - \frac{2\overline{m}b\!\left(\dfrac{x}{c_r}\right)\tau}{\beta (1 - r)(b^2 - 1)^{3/2}}(1 - ub)$$

$$= \overline{Q}\!\left(\overline{m}, r, \frac{x}{c_r}, u, b\right) = \overline{Q}_1 \qquad\qquad (1 \leqq u \leqq b) \qquad (19b)$$

For the superimposed supersonic-leading-edge delta wing

$$\frac{\Delta p}{q} = -\frac{1}{r} \, Q\!\left(\overline{m}, r, \frac{x}{c_r}, u, a\right) = -\frac{1}{r} \, Q_2 \qquad (0 \leqq u \leqq 1) \qquad\qquad (20a)$$

$$\frac{\Delta p}{q} = -\frac{1}{r} \, \overline{Q}\!\left(\overline{m}, r, \frac{x}{c_r}, u, a\right) = -\frac{1}{r} \, \overline{Q}_2 \qquad (1 \leqq u \leqq a) \qquad\qquad (20b)$$

The pressure field associated with the basic source distribution is shown in figure 4 for both the subsonic- and supersonic-leading-edge cases for particular wings. For these wings $\bar{m} = -\frac{1}{2}$ which prescribes that the maximum-thickness line, which is at the trailing edge, have maximum concavity (see fig. 3). The effect of having $\bar{m} < 0$ is that, as x/c_r increases, the pressures are progressively decreased in a spanwise direction below the values for a conical pressure field. If $\bar{m} > 0$, the pressures would be progressively increased in a spanwise direction above the conical pressures as x/c_r increases.

DRAG

For the drag of the delta wing herein considered, the following three distinct cases must be treated:

Case I - Supersonic leading edge and supersonic ridge line $(b > 1, a > 1)$

Case II - Subsonic leading edge and supersonic ridge line $(b < 1, a > 1)$

Case III - Subsonic leading edge and subsonic ridge line $(b < 1, a < 1)$

In computing the drag by the method of superposition, it must be kept in mind that the basic source distribution creates a pressure field the influence of which is felt over the whole surface of the wing; whereas the pressure field from the superimposed source distribution is felt only over that part of the wing which lies between the ridge lines and the trailing edge, except for case III where the pressure field "spills over" the ridge lines and exerts its influence on the forward slopes up to the Mach lines from the ridge-line apex.

Since the wings are symmetrical about both the x,y- and x,z-planes, the drag is computed for the right half of the upper surface of the wing and the result is then multiplied by four.

Case I.- The drag for case I (fig. 5(a)) is represented by

$$\frac{D}{q} = \int_S \frac{\Delta p}{q} \lambda \, dS \tag{21}$$

which, as a result of the superposition of source distributions, becomes

$$\frac{D}{4q} = \int_{A_1} Q_1\lambda_1 \ dS + \int_{B_1+B_2} Q_1\lambda_2 \ dS -$$

$$\frac{1}{r} \int_{B_1} Q_2\lambda_2 \ dS + \int_{A_2} \overline{Q}_1\lambda_1 \ dS +$$

$$\int_{B_3} \overline{Q}_1\lambda_2 \ dS - \frac{1}{r} \int_{B_2+B_3} \overline{Q}_2\lambda_2 \ dS \qquad (22)$$

The limits of integration on the second and fifth integrals make the operation rather cumbersome. This difficulty may be obviated by rewriting equation (22) in the following form, which includes the sub-stitution $\lambda_2 = -\dfrac{1-r}{r} \lambda_1$:

$$\frac{D}{4q} = \frac{1}{r} \int_{A_1} Q_1\lambda_1 \ dS - \frac{1-r}{r} \int_{A_1+B_1+B_2} Q_1\lambda_1 \ dS +$$

$$\frac{1-r}{r^2} \int_{B_1} Q_2\lambda_1 \ dS + \frac{1}{r} \int_{A_2} \overline{Q}_1\lambda_1 \ dS -$$

$$\frac{1-r}{r} \int_{A_2+B_3} \overline{Q}_1\lambda_1 \ dS + \frac{1-r}{r^2} \int_{B_2+B_3} \overline{Q}_2\lambda_1 \ dS \qquad (23)$$

For this case $b > 1$, $a > 1$.

The element of area is $dS = dx \ dy$, but the variables of integration are x and u where $u = \beta\dfrac{y}{x}$. Therefore, if $y = u\dfrac{x}{\beta}$ and the Jacobian of x and y is taken with respect to x and u, the element of area becomes $dS = \dfrac{x}{\beta} dx \ du$. Performing the operations indicated in equa-tion (23), reducing the result to coefficient form, and making the sub-stitution $a = \dfrac{b}{r}$ yields

$$\frac{C_D\beta}{\tau^2} = F_1(r,b) + \overline{m}F_2(r,b) + \overline{m}^2F_3(r,b) \qquad (b > 1 > r) \qquad (24)$$

Equations for F_1, F_2, and F_3 are given in appendix B and are plotted in figure 6.

Case II.- The drag for case II (fig. 5(b)) is given by

$$\frac{D}{4q} = \int_A P_1\lambda_1 \ dS + \int_{B_1+B_2} P_1\lambda_2 \ dS - \frac{1}{r}\int_{B_1} Q_2\lambda_2 \ dS - \frac{1}{r}\int_{B_2} \overline{Q}_2\lambda_2 \ dS$$

$$= \frac{1}{r}\int_A P_1\lambda_1 \ dS - \frac{1-r}{r}\int_{A+B_1+B_2} P_1\lambda_1 \ dS + \frac{1-r}{r^2}\int_{B_1} Q_2\lambda_1 \ dS +$$

$$\frac{1-r}{r^2}\int_{B_2} \overline{Q}_2\lambda_1 \ dS \qquad (25)$$

In evaluating equation (25) it must be remembered that $b < 1$, $a > 1$. The final value may be expressed in coefficient form by

$$\frac{C_D\beta}{\tau^2} = G_1(r,b) + \overline{m}G_2(r,b) + \overline{m}^2G_3(r,b) \qquad (1 > b > r) \qquad (26)$$

Equations for G_1, G_2, and G_3 are given in appendix B and plotted in figure 7 with the H-functions which are presented subsequently.

Case III.- The drag for case III (fig. 5(c)) is expressed as

$$\frac{D}{4q} = \int_{A_1+A_2} P_1\lambda_1 \ dS + \int_B P_1\lambda_2 \ dS - \frac{1}{r}\int_B P_2\lambda_2 \ dS - \frac{1}{r}\int_{A_2} P_2\lambda_1 \ dS$$

$$= \frac{1}{r}\int_{A_1+A_2} P_1\lambda_1 \ dS - \frac{(1-r)}{r}\int_{A_1+A_2+B} P_1\lambda_1 \ dS + \frac{(1-r)}{r^2}\int_B P_2\lambda_1 \ dS -$$

$$\frac{1}{r}\int_{A_2} P_2\lambda_1 \ dS \qquad (27)$$

Here $b < 1$, $a < 1$, and the result is

$$\frac{C_{D\beta}}{\tau^2} = H_1(r,b) + \bar{m}H_2(r,b) + \bar{m}^2 H_3(r,b) \qquad (1 > r > b) \qquad (28)$$

Equations for H_1, H_2, and H_3 are given in appendix B and plotted in figure 7.

Whether a variable-thickness-ratio delta wing is better from the wave-drag standpoint than a constant-thickness-ratio delta wing depends upon the criterion chosen. Equations (24), (26), and (28) give the drag for a constant-thickness-ratio delta wing when $\bar{m} = 0$; the results are identical to those of reference 1. Inasmuch as $F_2 > F_3$, $G_2 > G_3$, and $H_2 > H_3$ always, it is obvious that, if the variable- and constant-thickness-ratio wings are compared on the basis of identical plan form, r,b, and thickness ratio at the root, the concave thickness-distribution curve $\left(-\frac{1}{2} \leqq \bar{m} < 0, \text{ see fig. 3}\right)$ will give lower drag. This criterion, however, is a poor one because the internal volume and the projected frontal area are reduced. Since the same projected frontal area appears to provide a fair basis for comparison and internal volume is important in practical design considerations, these two criteria are developed for the purpose of comparing the drag of a constant- with a variable-thickness-ratio delta wing.

PROJECTED-FRONTAL-AREA CRITERION

If a variable-thickness-ratio delta wing and a constant-thickness-ratio delta wing have identical plan form, r, b, and projected frontal area, then

$$A_f = 2 \int_0^{c_r \epsilon_{LE}} t(y)\,dy$$

and from equation (15b)

$$t(y) = t_r \left(1 + \frac{2\bar{m} - 1}{c_r \epsilon_{LE}} y - \frac{2\bar{m}}{c_r^2 \epsilon_{LE}^2} y^2\right)$$

Therefore,

$$A_f = S\tau\left(1 + \frac{2}{3}\,\overline{m}\right) \tag{29}$$

where A_f is the projected frontal area, S is the plan-form area, and τ is the thickness ratio at the root.

For a constant-thickness-ratio delta wing

$$A_f{}' = S'\tau' \tag{30}$$

From equations (29) and (30), the stipulation that $A_f = A_f{}'$ and $S = S'$ gives the relationship between τ' and τ as

$$\tau' = \tau\left(1 + \frac{2}{3}\,\overline{m}\right) \tag{31}$$

From equation (24)

$$\frac{C_D\beta}{\tau^2} = F_1 + \overline{m}F_2 + \overline{m}^2F_3$$

for the variable-thickness-ratio delta wing, and

$$\frac{C_D{}'\beta}{\tau'^2} = F_1 \tag{32}$$

for the constant-thickness-ratio delta wing. Forming the ratio of equation (24) to equation (32) and substituting equation (31) gives:

$$\frac{C_D}{C_D{}'} = \frac{F_1 + \overline{m}F_2 + \overline{m}^2F_3}{\left(1 + \frac{2}{3}\,\overline{m}\right)^2 F_1} \tag{33}$$

The ratio $C_D/C_D{}'$ can be minimized with respect to $\bar{m}$, and the value of $\bar{m}$, which gives minimum drag for the conditions stipulated, is

$$\bar{m} = \frac{4F_1 - 3F_2}{6F_3 - 2F_2} \tag{34}$$

Equation (34) applies to the G- and H-functions as well as to the F-functions where the corresponding G- and H-functions are substituted for the F-functions.

The nondimensional thickness-distribution parameter $\bar{m}$ for minimum drag, based on frontal-area considerations, is presented in figure 8. Figure 9 presents $C_D/C_D{}'$ as calculated from equation (33) using the values of $\bar{m}$ obtained from figure 8. When $b > 1 > r$, it can be seen from figure 8 that the wing for minimum drag is essentially that with constant thickness ratio ($\bar{m} \approx 0$), except when $b = 1.001$, and even for this case figure 9 shows a maximum drag reduction of less than 2 percent.

When $1 > b > r$, figure 8 indicates that the wing for minimum drag has a concave thickness distribution ($\bar{m} < 0$). The corresponding curves of figure 9 indicate a maximum drag reduction of only about 4 percent for this case. The main conclusion to be drawn then is that, with the projected frontal area held constant, the thickness can be shifted from the tip to the root with no penalty in wave drag.

When $1 > r > b$, the optimum thickness distribution is sometimes concave ($\bar{m} < 0$, for which the same conclusion can be drawn as for $1 > b > r$) and sometimes convex ($\bar{m} > 0$). Some of the indicated shapes for $\bar{m} > 0$ are highly unrealistic $\left(\text{that is, } \bar{m} \gg \frac{1}{2}\right)$ which indicates that, within the realm of physically practical shapes, there is no minimum $\bar{m}$. This condition, however, does not mean that a drag reduction is not possible. Figure 10 presents the curve of $C_D/C_D{}'$ plotted against $\bar{m}$ for a case when $\bar{m}$, as determined from equation (34), gives an unrealistic shape. It can be seen that, although $\bar{m}$ for minimum drag as calculated from equation (34) is 3.68, values of $\bar{m}$ from 1/2 to 1 give a drag reduction of 20 to 25 percent. In figure 9 the dashed lines show values of $C_D/C_D{}'$ when $\bar{m}$ represents a wing that is unrealistic, where an unrealistic wing has arbitrarily been chosen to be one for which $\bar{m} > 1$. (See fig. 3.)

INTERNAL-VOLUME CRITERION

In order to compare the variable- and constant-thickness-ratio delta wings on the basis of internal volume, both wings are specified to have identical plan form, r, b, and internal volume. The internal volume of the wing of figure 1 is

$$V_i = \iint z \ dx \ dy \tag{35}$$

For the right half of the wing, from the leading edge to the ridge line

$$z = \frac{\frac{t(y)}{c(y)}\left(x - \frac{y}{\epsilon_{LE}}\right)}{1 - r} \tag{36}$$

and from the ridge line to the trailing edge

$$z = \frac{\frac{t(y)}{c(y)}\left(c_r - x\right)}{r} \tag{37}$$

Using equations (35), (36), and (37) gives, for a variable-thickness-ratio wing,

$$V_i = \frac{\tau c_r S}{3}\left(1 + \frac{1}{2}\ \overline{m}\right) \tag{38}$$

and for a constant-thickness-ratio wing

$$V_i{}' = \frac{\tau' c_r{}' S'}{3} \tag{39}$$

When equations (38) and (39) are equated and the conditions that $V_i = V_i{}'$, $c_r = c_r{}'$, and $S = S'$ are fulfilled,

$$\tau' = \tau \left(1 + \frac{1}{2} \bar{m}\right) \qquad (40)$$

Forming the ratio of $\dfrac{C_D\beta}{\tau^2}$ to $\dfrac{C_D'\beta}{\tau'^2}$, as before for the present criterion, gives

$$\frac{C_D}{C_D'} = \frac{F_1 + \bar{m}F_2 + \bar{m}^2 F_3}{\left(1 + \frac{1}{2} \bar{m}\right)^2 F_1} \qquad (41)$$

which, when minimized with respect to $\bar{m}$, gives

$$\bar{m} = 2 \frac{F_1 - F_2}{4F_3 - F_2} \qquad (42)$$

for the value of $\bar{m}$ for minimum drag under the conditions stipulated.

Values of $\bar{m}$ for minimum drag based on internal-volume considerations are presented in figure 11. Figure 12 presents C_D/C_D' as calculated from equation (41) by the use of the values of $\bar{m}$ from figure 11. When $b > 1 > r$, figure 11(b) shows that the value of $\bar{m}$ for minimum drag is approximately constant at about $\bar{m} = -0.45$; that is, the thickness distribution for minimum drag is very close to that of maximum concavity. The corresponding curve of figure 12 gives a maximum drag reduction of between 8 and 10 percent.

When $1 > b > r$, figure 11(a) indicates a value of $\bar{m}$ which is fictitious in that $\bar{m} < -\frac{1}{2}$ which would prescribe a wing where part of the upper surface is below the bottom surface and conversely. Therefore, there is no minimum drag for any real wings in this range. Figure 13 is a plot of C_D/C_D' against $\bar{m}$ for a particular configuration in this range. Although the optimum $\bar{m}$ as determined from equation (42) is fictitious, it can be seen that any value of $\bar{m}$ between $\bar{m} = -\frac{1}{2}$ and $\bar{m} = 0$ will give a drag reduction, the reduction in drag at $\bar{m} = -\frac{1}{2}$ being about 20 percent. In figure 12, the values of C_D/C_D' which were obtained by using fictitious values of $\bar{m}$ are represented by short dashed lines.

When $1 > r > b$, figure 11 shows that the $\bar{m}$ for minimum drag varies from negative to positive with increasing r for each value of b. Included in this range are both fictitious $\left(\bar{m} < -\frac{1}{2}\right)$ and unrealistic $\left(\bar{m} \gg \frac{1}{2}\right)$ values of $\bar{m}$ calculated from equation (42). The corresponding values of C_D/C_D' are shown in figure 12 where the short dashed lines were obtained by the use of fictitious values of $\bar{m}$ $\left(\bar{m} < -\frac{1}{2}\right)$ and the long dashed lines indicate the use of unrealistic values of $\bar{m}$ $(\bar{m} > 1)$. It should be emphasized, however, that substantial drag decreases can be realized in the regions of the dashed curves for practical wings, as can be seen from figures 10 and 13, which indicate the trend of all curves of C_D/C_D' plotted against $\bar{m}$ when the $\bar{m}$ for minimum C_D/C_D' is either positive or negative.

ILLUSTRATIVE EXAMPLE

If, for a given constant-thickness-ratio delta wing, it is desired to increase the thickness of the root and, for structural reasons, the thickness at the tip is not to be decreased, two methods are suggested. Either a variable-thickness-ratio wing with prescribed root and tip thickness ratios or a new constant-thickness-ratio wing with prescribed root thickness ratio could be formed.

For the former case, if τ' is the thickness ratio of the original constant-thickness-ratio wing, the slope of the maximum thickness line with respect to y is $-\tau'/2\epsilon_{LE}$. If the variable-thickness-ratio wing has this slope at the tip, equation (15) gives

$$\frac{\partial}{\partial y}\left[\frac{t(y)}{2}\right]_{y=c_r\epsilon_{LE}} = -\frac{\tau}{2\epsilon_{LE}}(1 + 2\bar{m}) = -\frac{\tau'}{2\epsilon_{LE}}$$

or

$$\tau' = \tau(1 + 2\bar{m}) \tag{43}$$

If the root thickness of the original wing is increased by n times,

$$\tau = n\tau' \qquad\qquad (44)$$

The two equations (43) and (44) yield the necessary thickness distribution

$$\bar{m} = \frac{1 - n}{2n} \qquad\qquad (45)$$

As an example, consider the wings for which $b = 0.8$ and $r = 0.5$. If the root thickness of the original constant-thickness-ratio wing is increased by 1/2, $n = \frac{3}{2}$ and $\bar{m} = -\frac{1}{6}$. When the ratio

$$\frac{c_D}{c_D'} = \frac{G_1 + \bar{m}G_2 + \bar{m}^2 G_3}{(1 + 2\bar{m})^2 G_1}$$

is formed, the drag of the variable-thickness-ratio wing is found to be 1.77 times that of the original constant-thickness-ratio wing.

If the increased root thickness is attained by forming a new constant-thickness-ratio wing, the drag is 2.25 times that of the original wing. Here, of course, both the projected frontal area and the internal volume are larger than those for the variable-thickness-ratio wing. The drag of a constant-thickness-ratio wing which has the same projected frontal area as the previously mentioned variable-thickness-ratio wing is 1.78 times the drag of the original wing; whereas, the drag of a constant-thickness-ratio wing which has the same internal volume as the previously mentioned variable-thickness-ratio wing is 1.89 times that of the original wing.

CONCLUDING REMARKS

The variable-thickness-ratio delta wing has been compared with the constant-thickness-ratio delta wing under the conditions that they have identical projected frontal area and identical internal volume. For these conditions the optimum value of the thickness-distribution parameter has been determined. The wing shape given by this value, although not always practical or real, nonetheless gives an indication of the types of maximum-thickness-line distribution; that is, whether it should be convex, straight, or concave. From the analysis the following conclusions are drawn:

1. On the basis of fixed frontal area,

(a) When the leading edge and ridge line are both supersonic, the constant-thickness-ratio delta wing has essentially optimum wave-drag characteristics for all combinations of leading-edge semiapex angle and position of the ridge line.

(b) When the leading edge is subsonic and the ridge line is supersonic, the concave maximum-thickness distribution has the optimum wave-drag characteristics which, compared with a constant-thickness-ratio wing, gives greater thickness at the root and less thickness at the tip. It should be noted, however, that the drag reduction which can be realized in this range is small.

(c) When the leading edge and ridge line are both subsonic, as the ridge line moves forward from the sonic condition to the leading edge, the maximum-thickness distribution for optimum wave drag goes from concave to straight to convex. For the latter case, the drag decrease indicated is large and absurd values are approached as the ridge line approaches the leading edge.

2. On the basis of internal volume considerations, ·

(a) When the leading edge and ridge line are both supersonic, the concave maximum-thickness distribution has optimum wave-drag characteristics, the drag reduction being about 8 to 10 percent for all combinations of leading-edge semiapex angle and position of the ridge line.

(b) When the leading edge is subsonic and the ridge line is supersonic, the concave thickness distribution has the best wave-drag characteristics, with drag reductions of as much as 20 percent being predicted.

(c) When the leading edge and ridge line are both subsonic, as the ridge line moves forward from the sonic condition to the leading edge, the maximum-thickness line goes from concave to straight to convex; whereas the corresponding drag reductions range from about 20 percent to zero to absurd values.

Langley Aeronautical Laboratory,
    National Advisory Committee for Aeronautics,
        Langley Field, Va., October 1, 1952.

APPENDIX A

EVALUATION OF $\dfrac{\partial \phi_1}{\partial x}$ $\left(\beta \epsilon_{LE} < 1\right)$

Equation (7) is

$$(\phi_1)_R = -\frac{V}{\pi(1-r)}\int_0^y \int_{\eta/\epsilon_{LE}}^{x-\beta(y-\eta)} \frac{\left(\dfrac{t_r}{2c_r}+m\eta\right)d\xi\ d\eta}{\sqrt{(x-\xi)^2-\beta^2(y-\eta)^2}} -$$

$$\frac{V}{\pi(1-r)}\int_y^{\frac{\epsilon_{LE}(x+\beta y)}{1+\beta\epsilon_{LE}}} \int_{\eta/\epsilon_{LE}}^{x+\beta(y-\eta)} \frac{\left(\dfrac{t_r}{2c_r}+m\eta\right)d\xi\ d\eta}{\sqrt{(x-\xi)^2-\beta^2(y-\eta)^2}}$$

Let

$$\left|\frac{x-\xi}{\beta(y-\eta)}\right| = \cosh z$$

Then

$$(\phi_1)_R = -\frac{V}{\pi(1-r)}\int_0^y \left(\frac{t_r}{2c_r}+m\eta\right)d\eta \int_0^{\cosh^{-1}\left|\frac{x-\frac{\eta}{\epsilon_{LE}}}{\beta(y-\eta)}\right|} dz -$$

$$\frac{V}{\pi(1-r)}\int_y^{\frac{\epsilon_{LE}(x+\beta y)}{1+\beta\epsilon_{LE}}} \left(\frac{t_r}{2c_r}+m\eta\right)d\eta \int_0^{\cosh^{-1}\left|\frac{x-\frac{\eta}{\epsilon_{LE}}}{\beta(y-\eta)}\right|} dz$$

$$= -\frac{V}{\pi(1-r)}\int_0^y \left(\frac{t_r}{2c_r}+m\eta\right)\cosh^{-1}\left|\frac{x-\frac{\eta}{\epsilon_{LE}}}{\beta(y-\eta)}\right| d\eta -$$

$$\frac{V}{\pi(1-r)}\int_y^{\frac{\epsilon_{LE}(x+\beta y)}{1+\beta\epsilon_{LE}}} \cdot \left(\frac{t_r}{2c_r}+m\eta\right)\cosh^{-1}\left|\frac{x-\frac{\eta}{\epsilon_{LE}}}{\beta(y-\eta)}\right| d\eta$$

Differentiating $(\phi_1)_R$ with respect to x gives

$$\left(\frac{\partial \phi_1}{\partial x}\right)_R = -\frac{V \epsilon_{LE}}{\pi(1-r)} \int_0^{\frac{\epsilon_{LE}(x+\beta y)}{1+\beta \epsilon_{LE}}} \frac{\left(\frac{t_r}{2c_r} + m\eta\right)d\eta}{\sqrt{(x\epsilon_{LE} - \eta)^2 - \beta^2 \epsilon_{LE}^2(y-\eta)^2}}$$

By the use of equations (160) and (169) in reference 2, the following equation is obtained:

$$\left(\frac{\partial \phi_1}{\partial x}\right)_R = -\frac{V \epsilon_{LE}}{\pi(1-r)\sqrt{1-\beta^2\epsilon_{LE}^2}} \left\{\left[\frac{t_r}{2c_r} - \right.\right.$$

$$\frac{m\left(\beta^2 y \epsilon_{LE}^2 - x\epsilon_{LE}\right)}{1-\beta^2\epsilon_{LE}^2}\right]\left[\log_e\left|\frac{\beta(y - x\epsilon_{LE})}{\sqrt{(x^2 - \beta^2 y^2)(1-\beta^2\epsilon_{LE}^2)} + \beta^2 y \epsilon_{LE} - x}\right| - \right.$$

$$\left.\left.\frac{m\sqrt{x^2\epsilon_{LE}^2 - \beta^2\epsilon_{LE}^2 y^2}}{\sqrt{1-\beta^2\epsilon_{LE}^2}}\right]\right\}$$

Let $b = \beta\epsilon_{LE}$ and $u = \beta\frac{y}{x}$; then

$$\left(\frac{\partial \phi_1}{\partial x}\right)_R = -\frac{V \epsilon_{LE}}{\pi(1-r)\sqrt{1-b^2}} \left\{\left[\frac{t_r}{2c_r} - \right.\right.$$

$$\frac{m\left(buxe_{LE} - x\epsilon_{LE}\right)}{1-b^2}\right]\left[\log_e\left|\frac{b-u}{1-bu-\sqrt{(1-u^2)(1-b^2)}}\right| - \right.$$

$$\left.\left.\frac{mx\epsilon_{LE}\sqrt{1-u^2}}{\sqrt{1-b^2}}\right]\right\}$$

Using equation (6) gives:

$$\frac{\partial \phi_1}{\partial x} = -\frac{V\epsilon_{LE}}{\pi(1-r)\sqrt{1-b^2}}\left\{\frac{t_r}{2c_r}\log_e\left|\frac{b^2-u^2}{\left(\sqrt{1-u^2}-\sqrt{1-b^2}\right)^2}\right| + \right.$$

$$\frac{mx\epsilon_{LE}}{1-b^2}\log_e\left|\frac{b^2-u^2}{\left(\sqrt{1-u^2}-\sqrt{1-b^2}\right)^2}\right| - \frac{2mx\epsilon_{LE}\sqrt{1-u^2}}{\sqrt{1-b^2}} -$$

$$\left.\frac{mbux\epsilon_{LE}}{1-b^2}\log_e\left|\frac{(b-u)\left[1+bu-\sqrt{\left(1-u^2\right)\left(1-b^2\right)}\right]}{(b+u)\left[1-bu-\sqrt{\left(1-u^2\right)\left(1-b^2\right)}\right]}\right|\right\}$$

Finally, after some algebraic manipulations are made and the identity

$$\log_e\frac{1+x}{1-x} = 2\tanh^{-1}x \qquad\qquad (x^2 < 1)$$

is used, this equation is obtained in the following form:

$$\frac{\partial \phi_1}{\partial x} = -\frac{2V\left(\frac{t_r}{2c_r}\right)b}{\beta\pi(1-r)\sqrt{1-b^2}}\tanh^{-1}\frac{\sqrt{1-b^2}}{\sqrt{1-u^2}} -$$

$$\frac{2Vmb^2x}{\beta^2\pi(1-r)(1-b^2)^{3/2}}\tanh^{-1}\frac{\sqrt{1-b^2}}{\sqrt{1-u^2}} +$$

$$\frac{2Vmb^3ux}{\beta^2\pi(1-r)(1-b^2)^{3/2}}\tanh^{-1}\frac{u\sqrt{1-b^2}}{b\sqrt{1-u^2}} +$$

$$\frac{2Vmb^2x}{\beta^2\pi(1-r)(1-b^2)}\sqrt{1-u^2}$$

APPENDIX B

PRESENTATION OF F-, G-, AND H-FUNCTIONS

F-Functions $(b > 1 > r)$

$$F_1(r,b) = \frac{2}{\pi}\left[\frac{b}{(1-r^2)\sqrt{b^2-1}}\cos^{-1}\frac{1}{b} + \frac{2b}{r(1-r^2)\sqrt{b^2-r^2}}\tan^{-1}\frac{\sqrt{b^2-r^2}}{b-r}\right]$$

$$F_2(r,b) = \frac{8}{3\pi}\left\{\left[\frac{b(1+r)}{r(1-r^2)\sqrt{b^2-r^2}} + \frac{b(1-r)}{2(1-r^2)(b^2-r^2)^{3/2}}\right]\tan^{-1}\frac{\sqrt{b^2-r^2}}{b-r} - \right.$$

$$\frac{b(1-r)}{2(1-r^2)(b^2-1)^{3/2}}\cos^{-1}\frac{1}{b} +$$

$$\left. \frac{b^2-r}{2b(b^2-1)(b^2-r^2)} + \frac{b}{2r(1-r)\sqrt{b^2-r^2}}\cos^{-1}\frac{r}{b}\right\}$$

$$F_3(r,b) = \frac{4}{\pi}\left\{\left[\frac{b(1-r)(1+3r^2)}{3(1-r^2)^2(b^2-r^2)^{3/2}} - \frac{2b(1-r)^2(1+3r^2)}{3r(1-r^2)^3\sqrt{b^2-r^2}}\right]\tan^{-1}\frac{\sqrt{b^2-r^2}}{b-r} + \right.$$

$$\left[\frac{b(1-r)(3+r^2)}{6(1-r^2)^2(b^2-1)^{3/2}} - \right.$$

$$\left.\frac{b(1-r)^2(3+r^2)}{3(1-r^2)^3\sqrt{b^2-1}}\right]\cos^{-1}\frac{1}{b} + \frac{b^2-r}{6b(b^2-1)(b^2-r^2)} -$$

$$\left. \frac{2b(1-r)^2(b^2+r)}{3(1-r^2)^2(b^2-1)(b^2-r^2)} + \frac{\pi b(2b^2-3r^2)}{6r(1-r)(b^2-r^2)^{3/2}}\right\}$$

G-Functions $(1 > b > r)$

$$G_1(r,b) = \frac{2}{\pi} \left\{ \frac{b}{(1 - r^2)\sqrt{1 - b^2}} \left[\log_e b + \log_e \frac{b}{1 - \sqrt{1 - b^2}} \right] + \right.$$

$$\frac{2b}{r(1 - r^2)\sqrt{b^2 - r^2}} \tan^{-1} \frac{\sqrt{b^2 - r^2}}{1 - r + \sqrt{1 - b^2}} + \frac{1}{r(1 - r)} \cos^{-1} b \left. \right\}$$

$$G_2(r,b) = \frac{8}{3\pi} \left\{ \frac{b}{(1 - r^2)(1 - b^2)^{3/2}} \log_e b + \right.$$

$$\frac{b(1 - r)}{2(1 - r^2)(1 - b^2)^{3/2}} \log_e \frac{b}{1 - \sqrt{1 - b^2}} +$$

$$\left[\frac{b(1 - r)}{(1 - r^2)(b^2 - r^2)^{3/2}} + \right.$$

$$\left. \frac{b(1 + r)}{r(1 - r^2)\sqrt{b^2 - r^2}} \right] \tan^{-1} \frac{\sqrt{b^2 - r^2}}{1 - r + \sqrt{1 - b^2}} +$$

$$\frac{(1 + r)(b^2 - r)}{2b(1 - r^2)(b^2 - r^2)\sqrt{1 - b^2}} - \frac{b^2 - r}{2b(b^2 - r^2)(1 - b^2)} +$$

$$\frac{1}{2r(1 - r)} \cos^{-1} b + \frac{b}{2r(1 - r)\sqrt{b^2 - r^2}} \cos^{-1} \frac{r}{b} \left. \right\}$$

$$G_3(r,b) = \frac{4}{\pi} \left\{ -\left[\frac{4b(1-r)^2}{3(1-r^2)^3\sqrt{1-b^2}} + \frac{b^3(1-r)^2}{3(1-r^2)^2(1-b^2)^{3/2}} \right] \log_e b - \right.$$

$$\left[\frac{b(1-r)^2(3+r^2)}{3(1-r^2)^3\sqrt{1-b^2}} + \right.$$

$$\left. \frac{b(1-r)(3+r^2)}{6(1-r^2)^2(1-b^2)^{3/2}} \right] \log_e \frac{b}{1-\sqrt{1-b^2}} +$$

$$\left[\frac{2b(1-r)^2(3+r^2)}{3(1-r^2)^3\sqrt{b^2-r^2}} + \right.$$

$$\left. \frac{b(1-r)^2(1+r^2)}{3(1-r^2)^2(b^2-r^2)^{3/2}} \right] \tan^{-1} \frac{\sqrt{b^2-r^2}}{1-r+\sqrt{1-b^2}} +$$

$$\frac{(1-r)\left[2(1-b^2)-(b^2-r)\right]}{6b(1-r^2)^2\sqrt{1-b^2}} -$$

$$\frac{r(1-r)(1-b^4)}{6b(1-r^2)^2(b^2-r^2)\sqrt{1-b^2}} - \frac{b^2-r}{6b(b^2-r^2)(1-b^2)} +$$

$$\left. \frac{2b(1-r)^2(b^2+r)}{3(1-r^2)^2(b^2-r^2)(1-b^2)} + \frac{b(2b^2-3r^2)}{6r(1-r)(b^2-r^2)^{3/2}} \cos^{-1} \frac{r}{b} \right\}$$

H-Functions $(1 > r > b)$

$$H_1(r,b) = \frac{2}{\pi}\left\{\frac{b}{(1 - r^2)\sqrt{1 - b^2}}\left[\log_e b + \log_e \frac{b}{1 - \sqrt{1 - b^2}}\right] - \right.$$

$$\frac{b}{r(1 - r^2)\sqrt{r^2 - b^2}} \log_e \frac{(1 - r)\left(r + \sqrt{r^2 - b^2}\right)}{r - b^2 + \sqrt{(r^2 - b^2)(1 - b^2)}} -$$

$$\frac{1}{r(1 - r)} \sin^{-1} b + \frac{1}{r(1 - r)} \sin^{-1} \frac{b}{r} -$$

$$\frac{b}{r(1 - r^2)\sqrt{r^2 - b^2}} \log_e \frac{b}{r} +$$

$$\left.\frac{b}{(1 - r^2)\sqrt{1 - b^2}} \log_e \frac{b(1 - r)}{r - b^2 + \sqrt{(r^2 - b^2)(1 - b^2)}}\right\}$$

$$H_2(r,b) = \frac{8}{3\pi}\left\{\frac{b}{(1 - r^2)(1 - b^2)^{3/2}} \log_e b + \right.$$

$$\frac{b(1 - r)}{2(1 - r^2)(1 - b^2)^{3/2}} \log_e \frac{b}{1 - \sqrt{1 - b^2}} -$$

$$\frac{r - b^2}{2b(r^2 - b^2)(1 - b^2)} + \left[\frac{b(1 - r)}{2(1 - r^2)(r^2 - b^2)^{3/2}} - \right.$$

$$\left.\frac{b(1 + r)}{2r(1 - r^2)\sqrt{r^2 - b^2}}\right]\log_e \frac{(1 - r)\left(r + \sqrt{r^2 - b^2}\right)}{r - b^2 + \sqrt{(r^2 - b^2)(1 - b^2)}} -$$

$$\frac{1}{2r(1-r)}\sin^{-1}b + \frac{\left(r-b^2\right)(1+r)}{2b\left(1-r^2\right)\left(r^2-b^2\right)\sqrt{1-b^2}} -$$

$$\frac{br}{\left(1-r^2\right)\left(r^2-b^2\right)^{3/2}}\log_e\frac{b}{r} + \left[\frac{b(1+r)}{2r\left(1-r^2\right)\sqrt{1-b^2}} + \right.$$

$$\left.\frac{b(1-r)}{2\left(1-r^2\right)\left(1-b^2\right)^{3/2}}\right]\log_e\frac{b(1-r)}{r-b^2+\sqrt{\left(r^2-b^2\right)\left(1-b^2\right)}} +$$

$$\frac{b}{2r(1-r)\sqrt{r^2-b^2}}\log_e\frac{r+\sqrt{r^2-b^2}}{b} + \frac{1}{2r(1-r)}\sin^{-1}\frac{b}{r} -$$

$$\frac{r}{2b\left(1-r^2\right)\sqrt{r^2-b^2}} - \frac{r^2-b^2}{2b\left(1-r^2\right)\left(1-b^2\right)\sqrt{r^2-b^2}}\Bigg\}$$

$$H_3(r,b) = \frac{4}{\pi}\left\{\left[\frac{b(1-r)^2\left(1+r^2\right)}{6\left(1-r^2\right)^2\left(r^2-b^2\right)^{3/2}} - \right.\right.$$

$$\left.\frac{b(1-r)^2\left(3+r^2\right)}{3\left(1-r^2\right)^3\sqrt{r^2-b^2}}\right]\log_e\frac{(1-r)\left(r+\sqrt{r^2-b^2}\right)}{r-b^2+\sqrt{\left(r^2-b^2\right)\left(1-b^2\right)}} -$$

$$\left[\frac{b(1-r)\left(3+r^2\right)}{6\left(1-r^2\right)^2\left(1-b^2\right)^{3/2}} + \right.$$

$$\left.\frac{b(1-r)^2\left(3+r^2\right)}{3\left(1-r^2\right)^3\sqrt{1-b^2}}\right]\log_e\frac{b}{1-\sqrt{1-b^2}} -$$

$$\left[\frac{4b(1-r)^2}{3\left(1-r^2\right)^3\sqrt{1-b^2}} + \frac{b^3(1-r)^2}{3\left(1-r^2\right)^2\left(1-b^2\right)^{3/2}}\right]\log_e b -$$

$$\frac{r - b^2}{6b(r^2 - b^2)(1 - b^2)} + \frac{(1 - r)\left[2(1 - b^2) + (r - b^2)\right]}{6b(1 - r^2)^2\sqrt{1 - b^2}} +$$

$$\frac{r(1 - r)(1 - b^4)}{6b(1 - r^2)^2(r^2 - b^2)\sqrt{1 - b^2}} - \frac{2b(1 - r)^2(r + b^2)}{3(1 - r^2)^2(r^2 - b^2)(1 - b^2)} +$$

$$\left[\frac{4br(1 - r)^2}{3(1 - r^2)^3\sqrt{r^2 - b^2}} - \frac{b^3(1 - r)^2}{3r(1 - r^2)^2(r^2 - b^2)^{3/2}}\right]\log_e \frac{b}{r} +$$

$$\left[\frac{b(1 - r)^2(1 + r^2)}{6r(1 - r^2)^2(1 - b^2)^{3/2}} +\right.$$

$$\left.\frac{b(1 - r)^2(1 + 3r^2)}{3r(1 - r^2)^3\sqrt{1 - b^2}}\right]\log_e \frac{b(1 - r)}{r - b^2 + \sqrt{(r^2 - b^2)(1 - b^2)}} +$$

$$\frac{b(3r^2 - 2b^2)}{6r(1 - r)(r^2 - b^2)^{3/2}}\log_e \frac{r + \sqrt{r^2 - b^2}}{b} -$$

$$\frac{(1 - r)\left[2(r^2 - b^2) + (r - b^2)\right]}{6b(1 - r^2)^2\sqrt{r^2 - b^2}} - \frac{(1 - r)(r^4 - b^4)}{6br(1 - r^2)^2(1 - b^2)\sqrt{r^2 - b^2}}\right\}$$

REFERENCES.

1. Puckett, Allen E.: Supersonic Wave Drag of Thin Airfoils. Jour.
      Aero. Sci., vol. 13, no. 9, Sept. 1946, pp. 475-484.

2. Peirce, B. O.: A Short Table of Integrals. Third rev. ed., Ginn
      and Co., 1929.
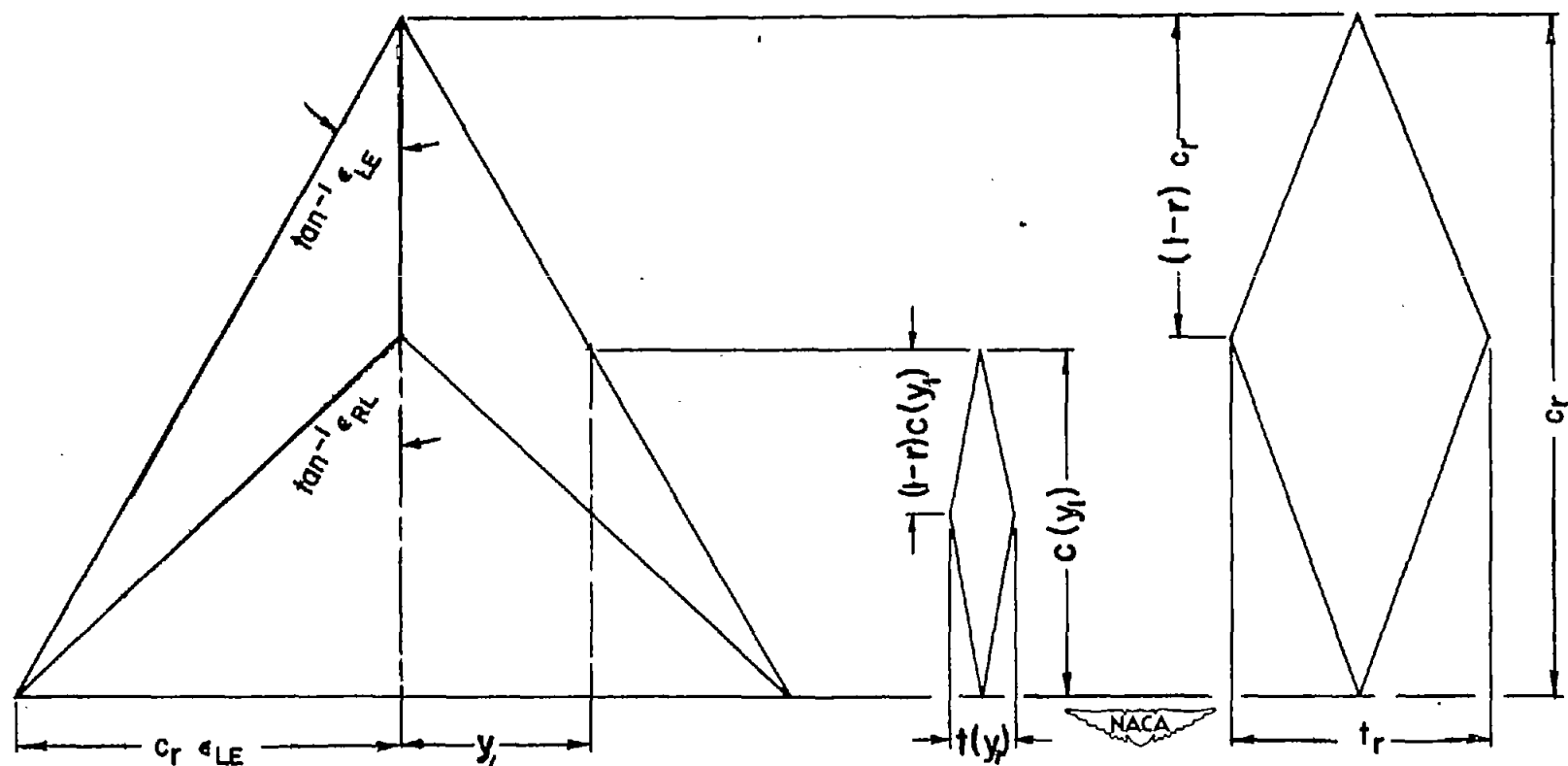
Figure 1.- Plan form and profiles of delta wing with varying thickness ratio.

(a) Subsonic leading edge
($\beta\epsilon < 1$).

(b) Supersonic leading edge
($\beta\epsilon > 1$).
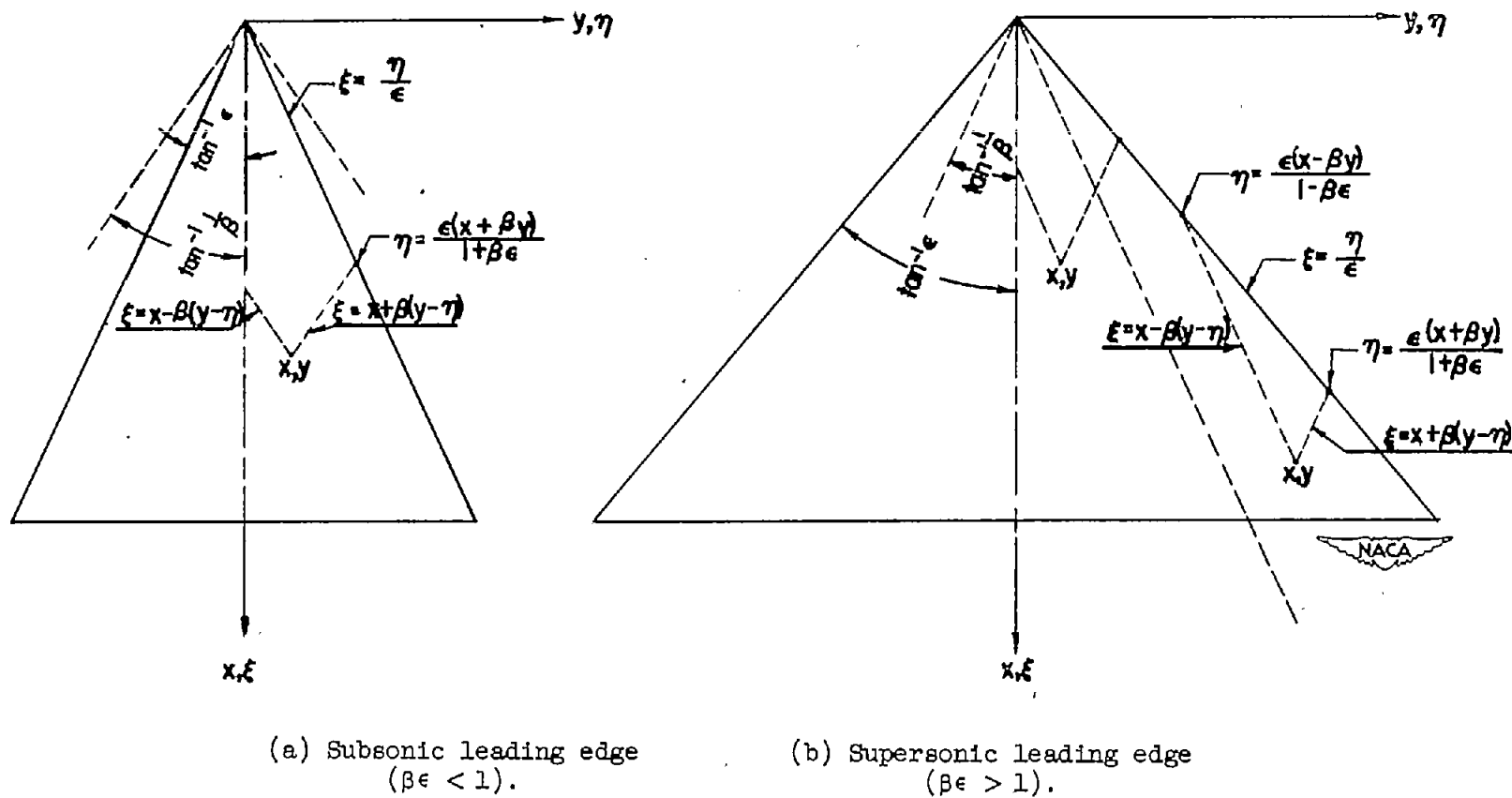
Figure 2.- Limits of integration for determining the potential due to a source distribution representing a subsonic- and supersonic-leading-edge wing.
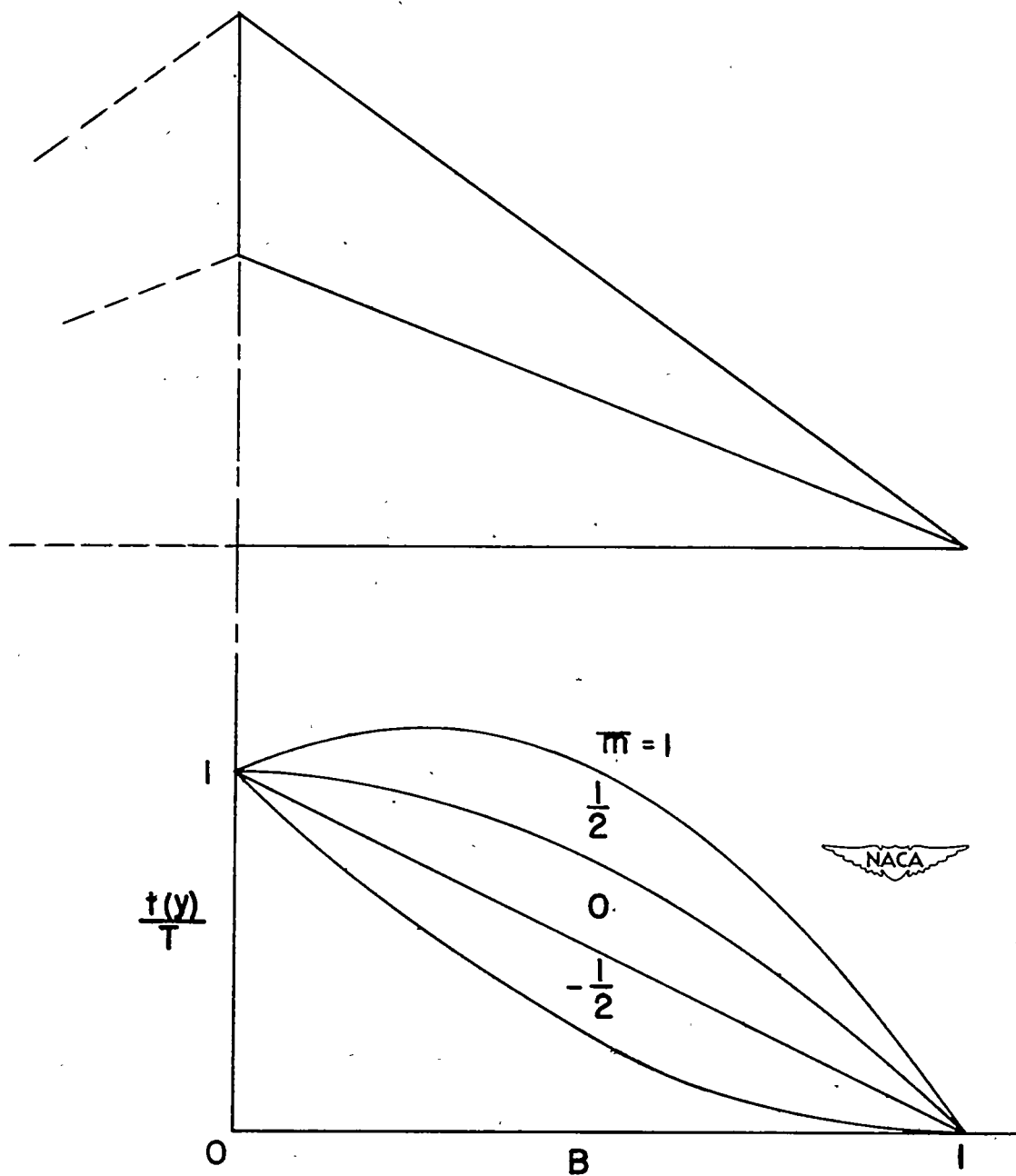
Figure 3.- Spanwise variation of thickness distribution for various
values of $\overline{m}$.
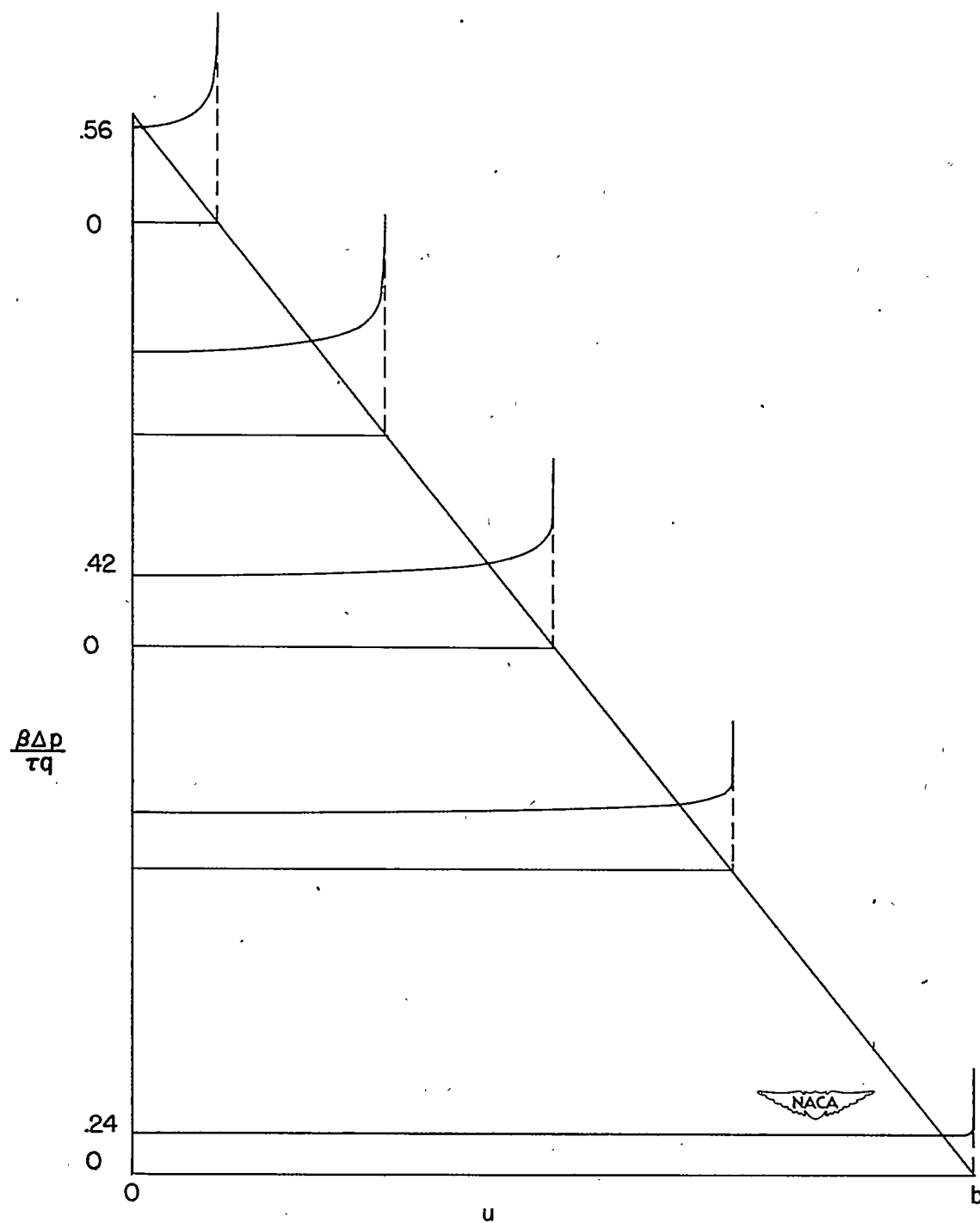
(a) Subsonic leading edge; $b = 0.2$, $r = 0.5$, and $\overline{m} = -\frac{1}{2}$.

Figure 4.- Variation of spanwise pressure distribution in the chordwise
direction for single-wedge-profile, variable-thickness-ratio delta
wings with subsonic and supersonic leading edges.
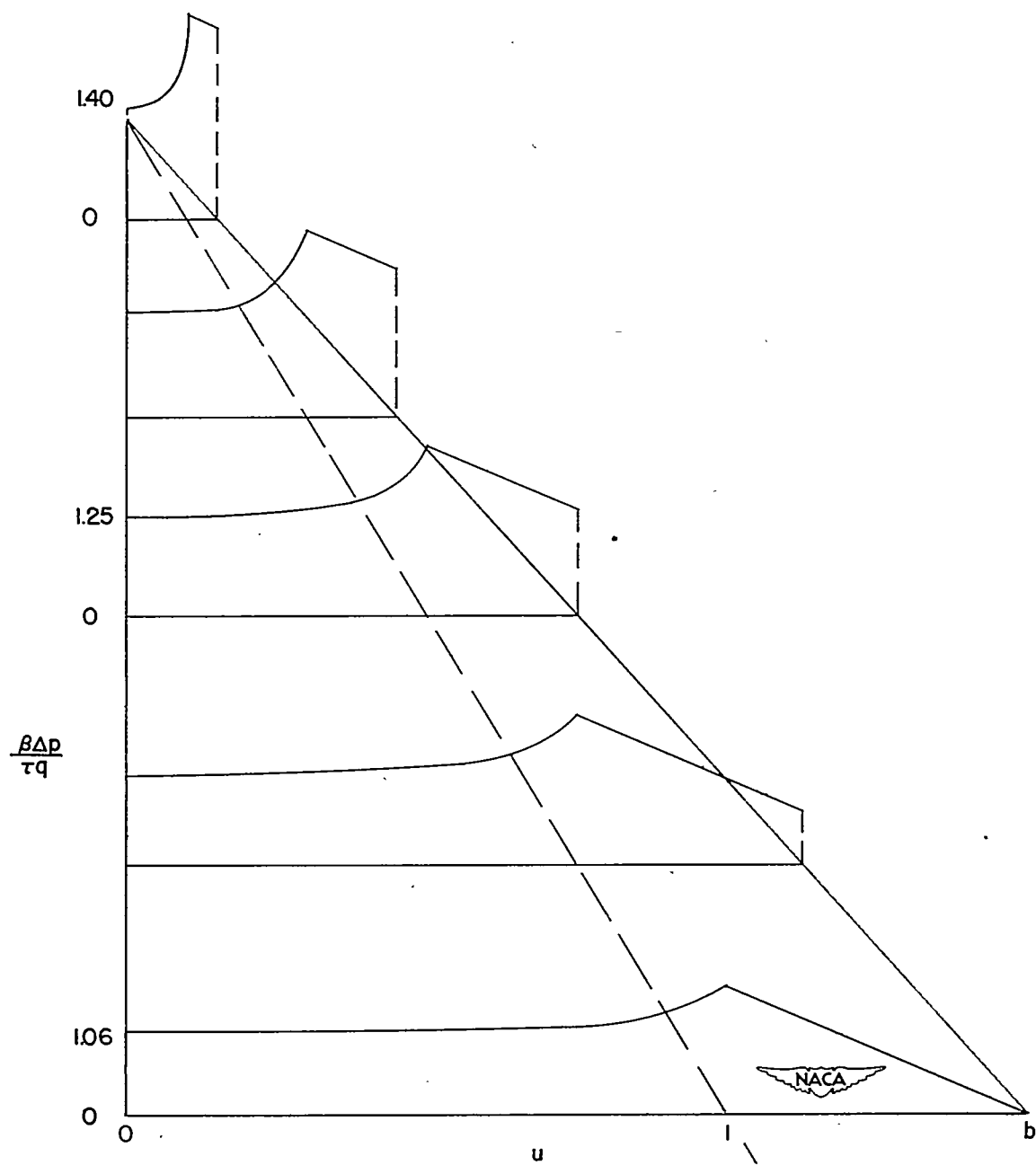
(b) Supersonic leading edge; $b = 1.5$, $r = 0.5$, and $\bar{m} = -\dfrac{1}{2}$.

Figure 4.- Concluded.
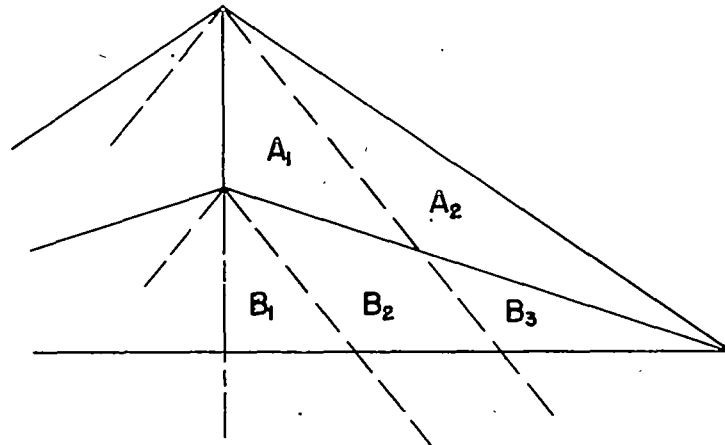
(a) Case I: $b > 1$, $a > 1$.
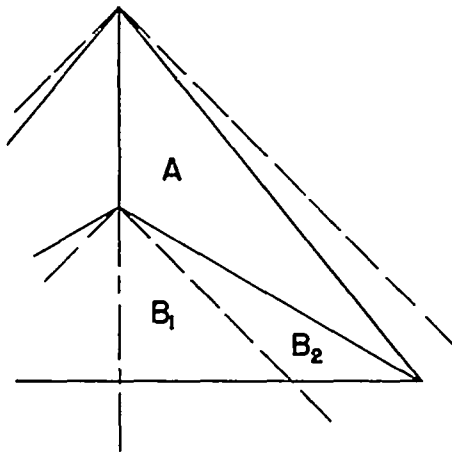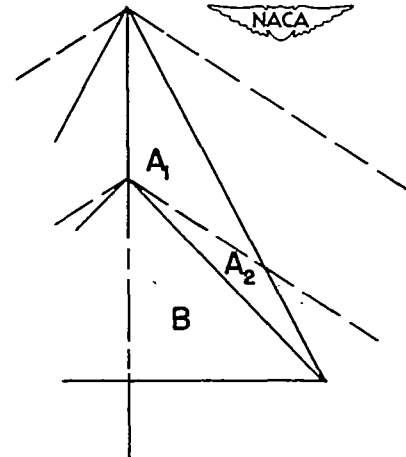
(b) Case II: $b < 1$, $a > 1$.   (c) Case III: $b < 1$, $a < 1$.

Figure 5.- Regions of integration for computing the drag.
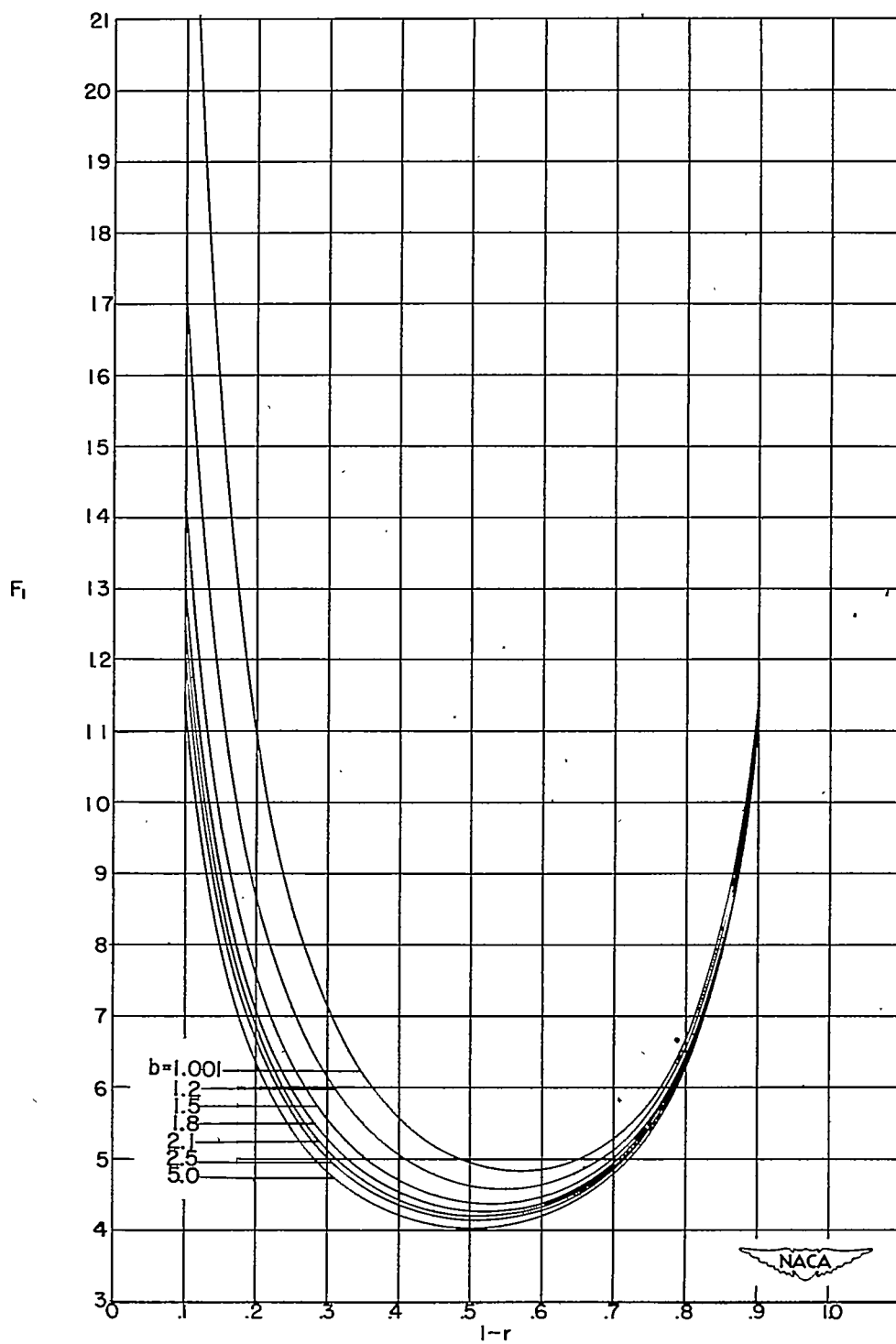
(a) $F_1(r,b)$.

Figure 6.- Variation of F-functions with $1 - r$ for different values of b.
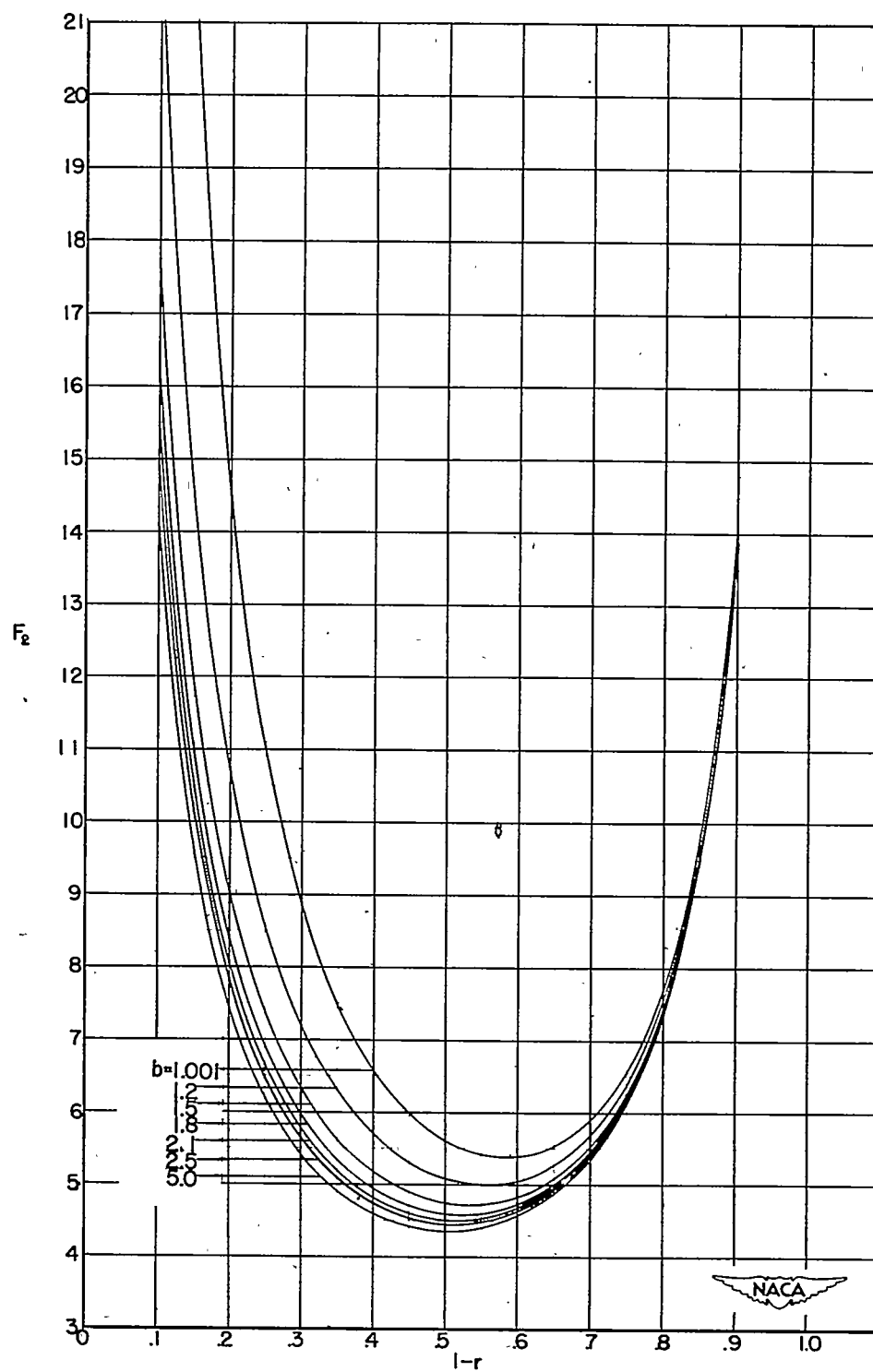
(b) $F_2(r,b)$.

Figure 6.- Continued.
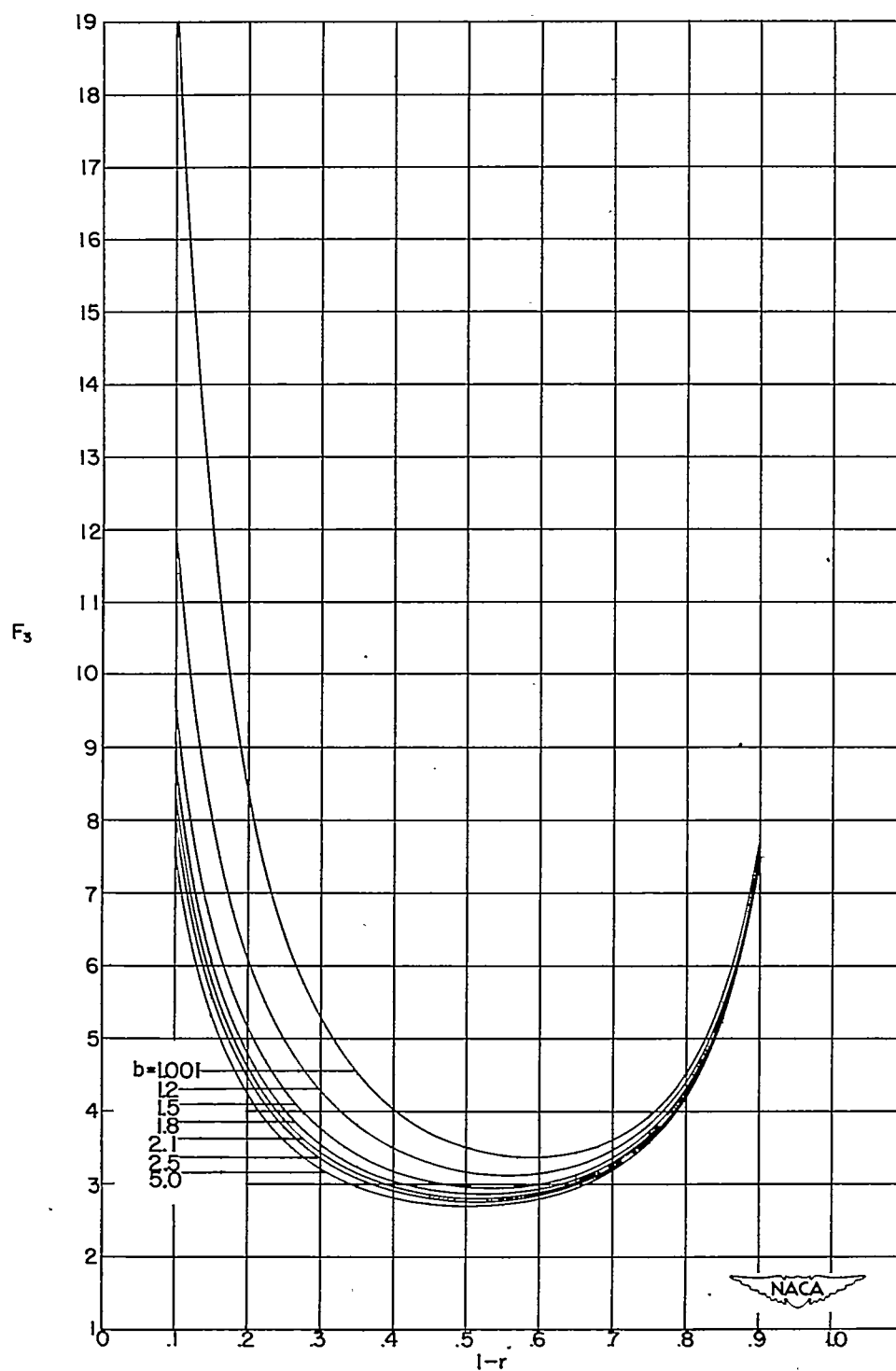
(c) $F_3(r,b)$.

Figure 6.- Concluded.
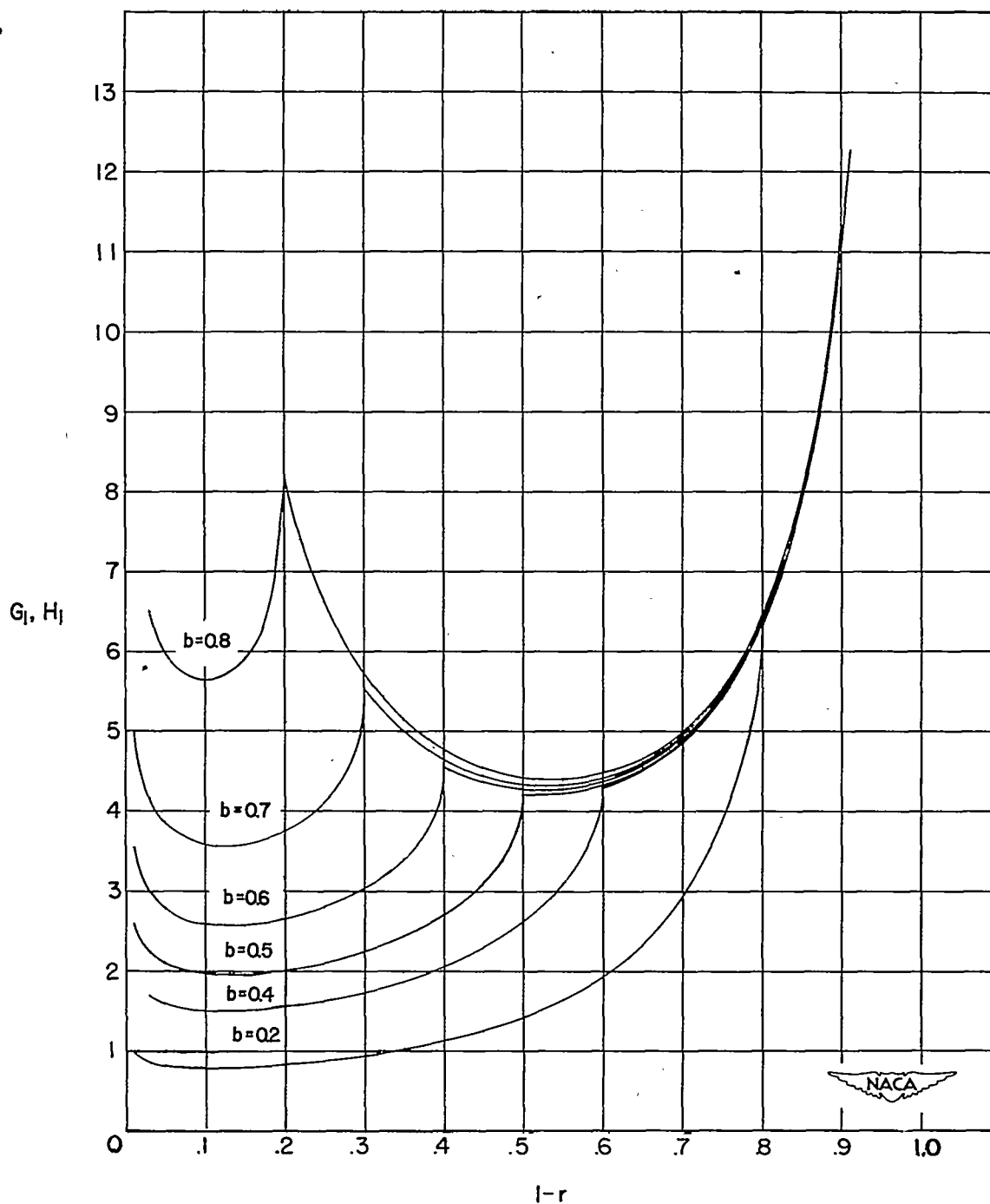
(a) $G_1(r,b)$ and $H_1(r,b)$. G-functions
are on the right of the cusp.

Figure 7.- Variation of G- and H-functions with 1 - r for different
values of b.
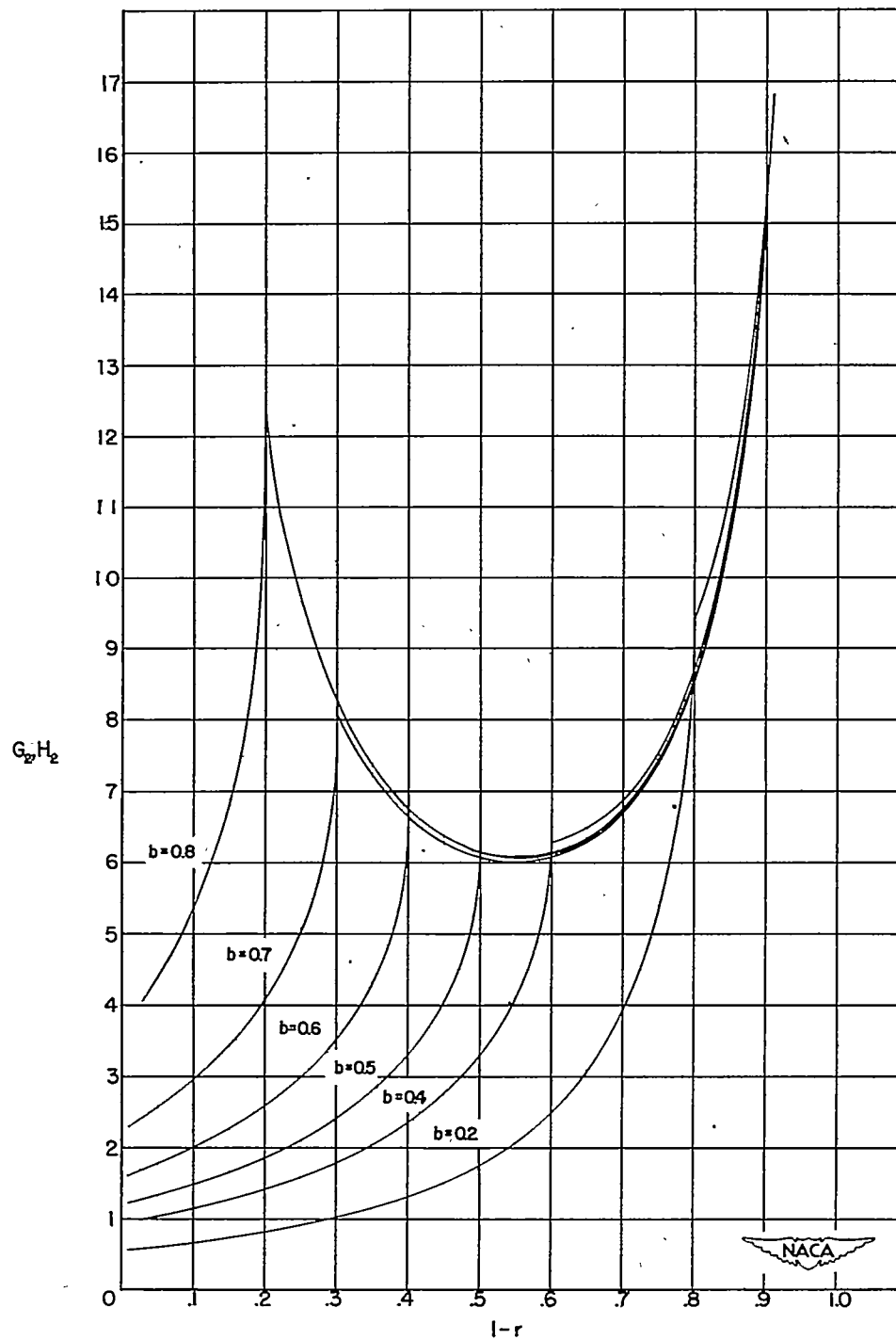
(b) $G_2(r,b)$ and $H_2(r,b)$. G-functions
are on the right of the cusp.

Figure 7.- Continued.
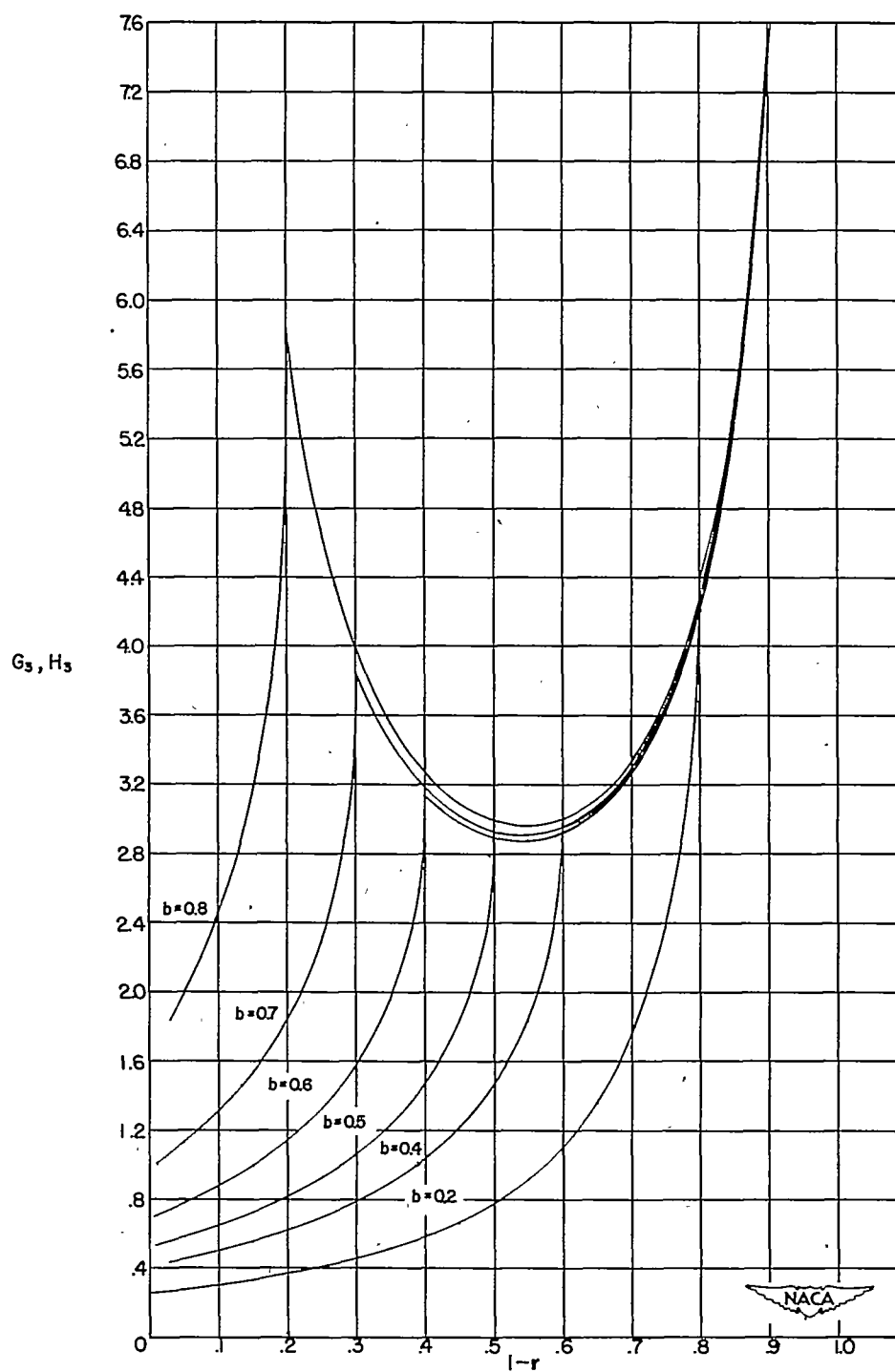
(c) $G_3(r,b)$ and $H_3(r,b)$. G-functions
are on the right of the cusp.

Figure 7.- Concluded.
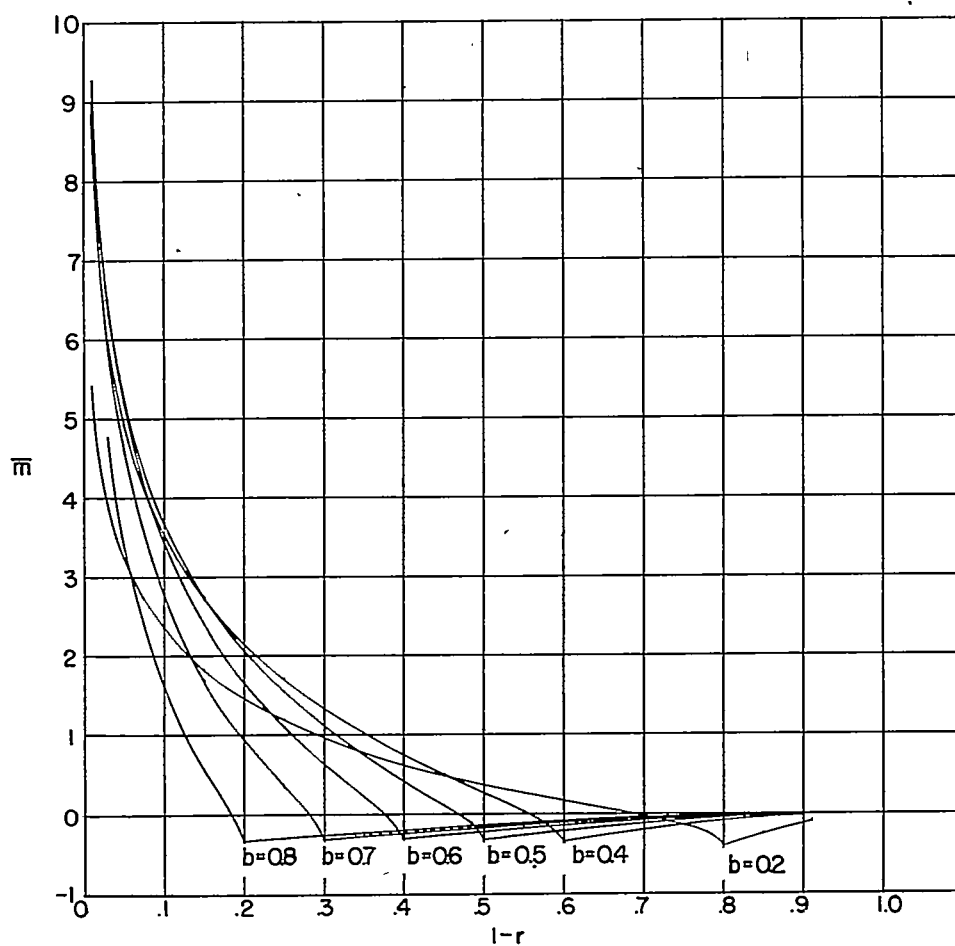
(a) $\overline{m}$ for G- and H-functions.
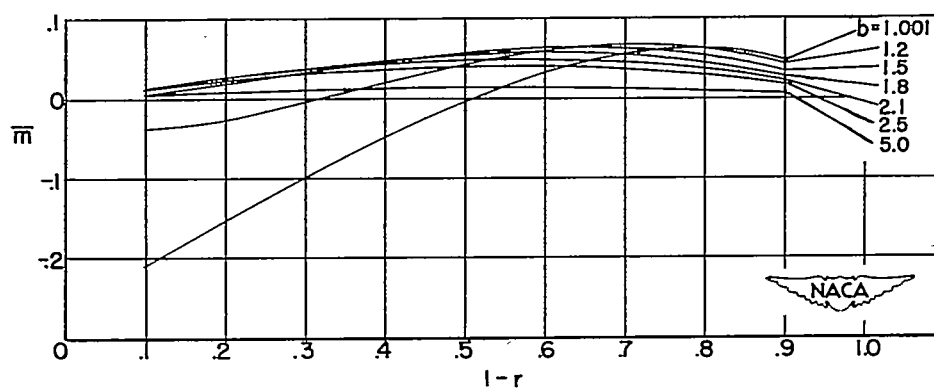
(b) $\overline{m}$ for F-functions.

Figure 8.- Variation of $\overline{m}$ for minimum C_D/C_D' based on projected-frontal-area considerations with $1 - r$ for different values of b.
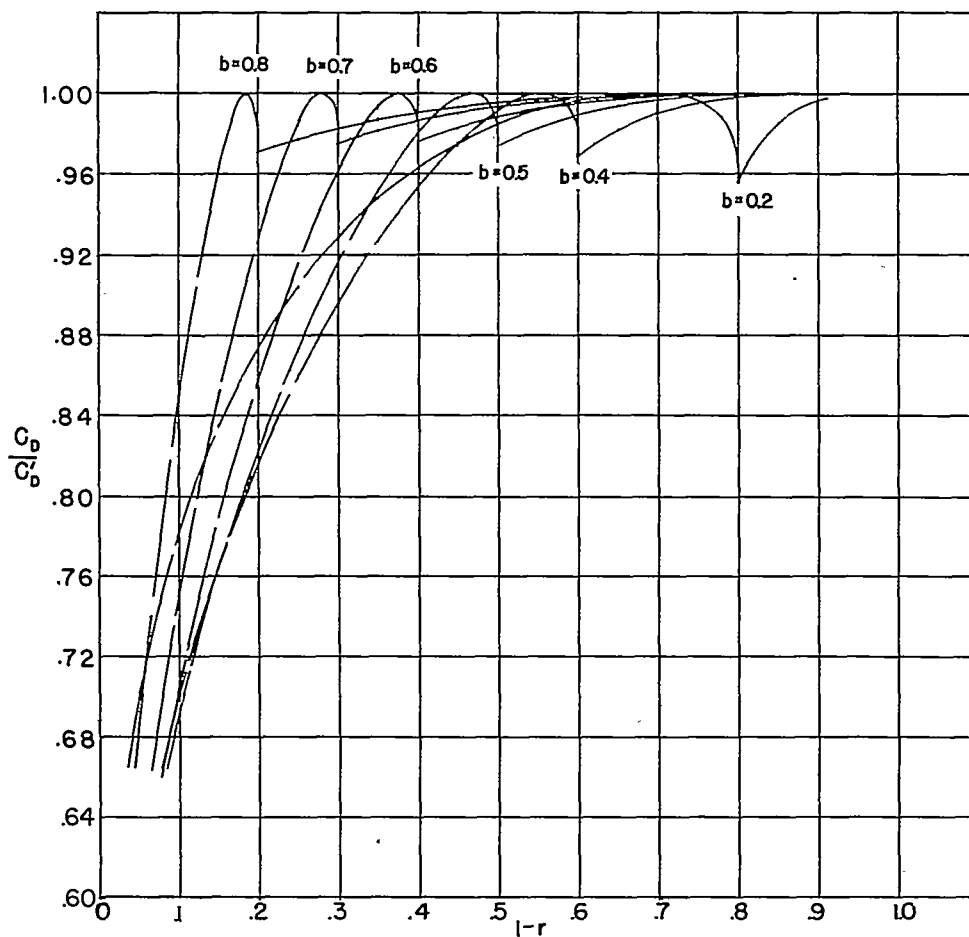
(a) C_D/C_D' for G- and H-functions.
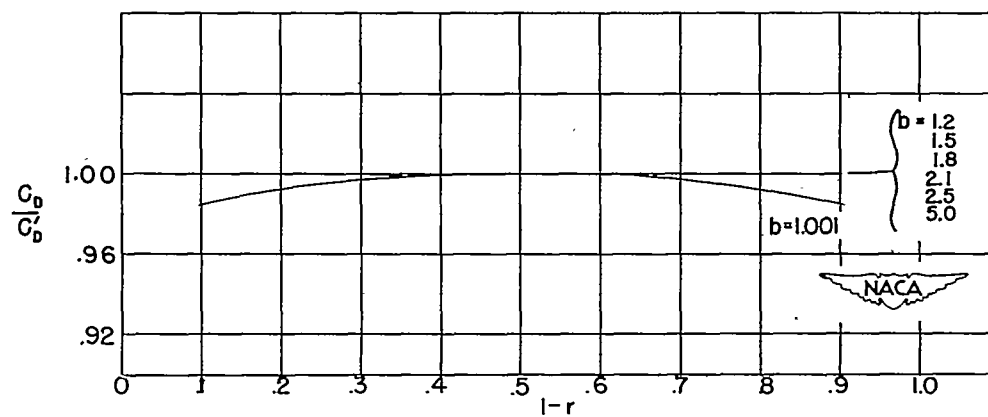
(b) C_D/C_D' for F-functions.

Figure 9.- Variation of C_D/C_D' with $1 - r$ for different values of b using the values of $\bar{m}$ from figure 8.
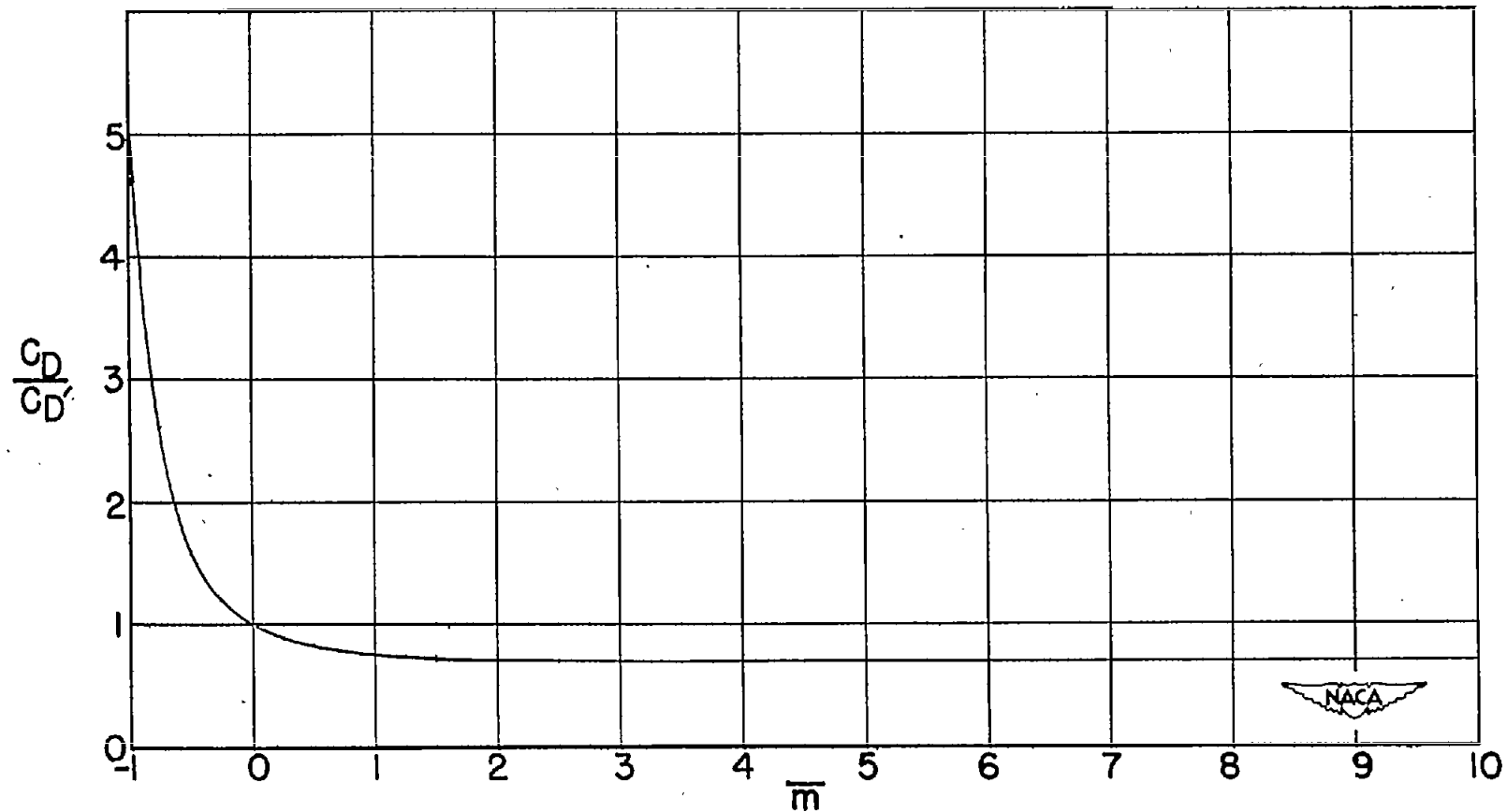
Figure 10.- Variation of C_D/C_D' with $\bar{m}$ for a case when $\bar{m}$ for minimum C_D/C_D' prescribes an impractical maximum thickness distribution. $b = 0.5$, $r = 0.9$.
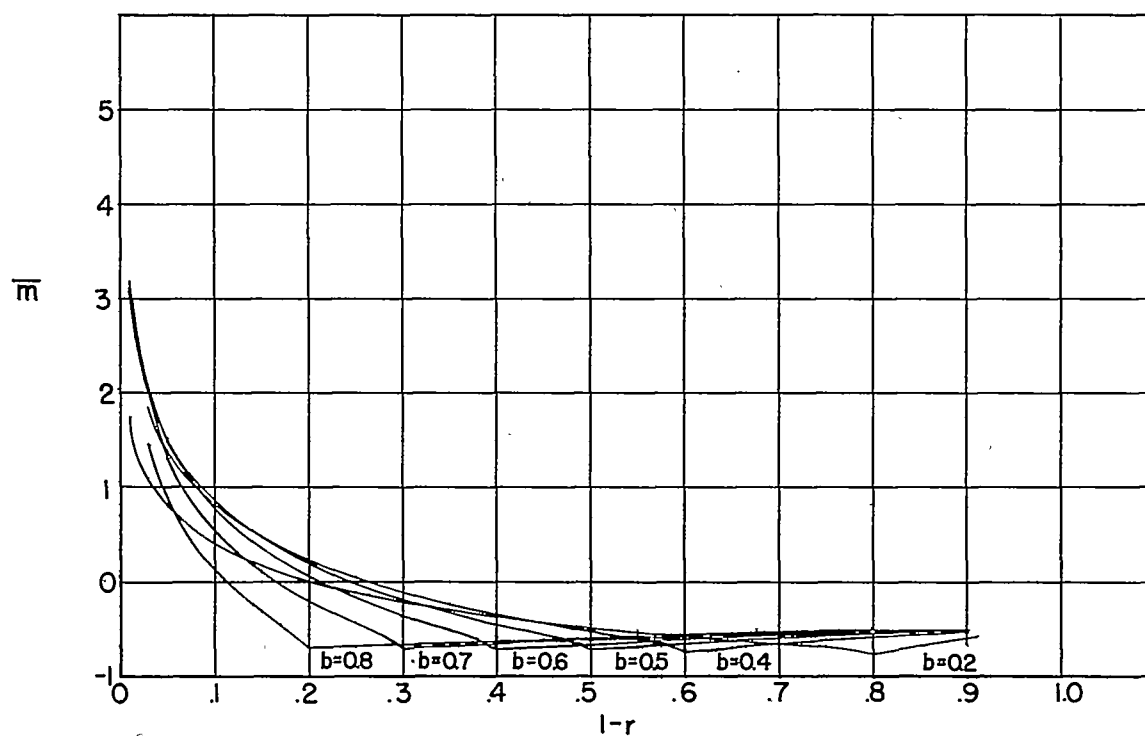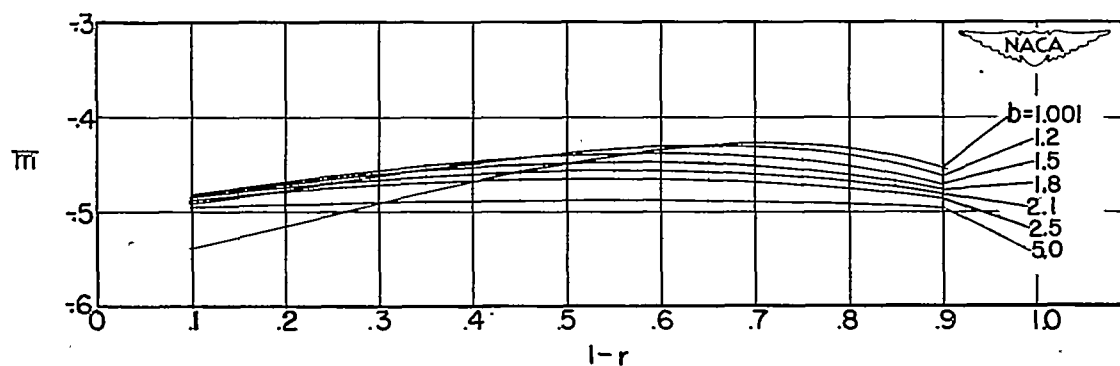
(a) $\bar{m}$ for G- and H-functions.

(b) $\bar{m}$ for F-functions.

Figure 11.- Variation of $\bar{m}$ for minimum C_D/C_D' based on internal-
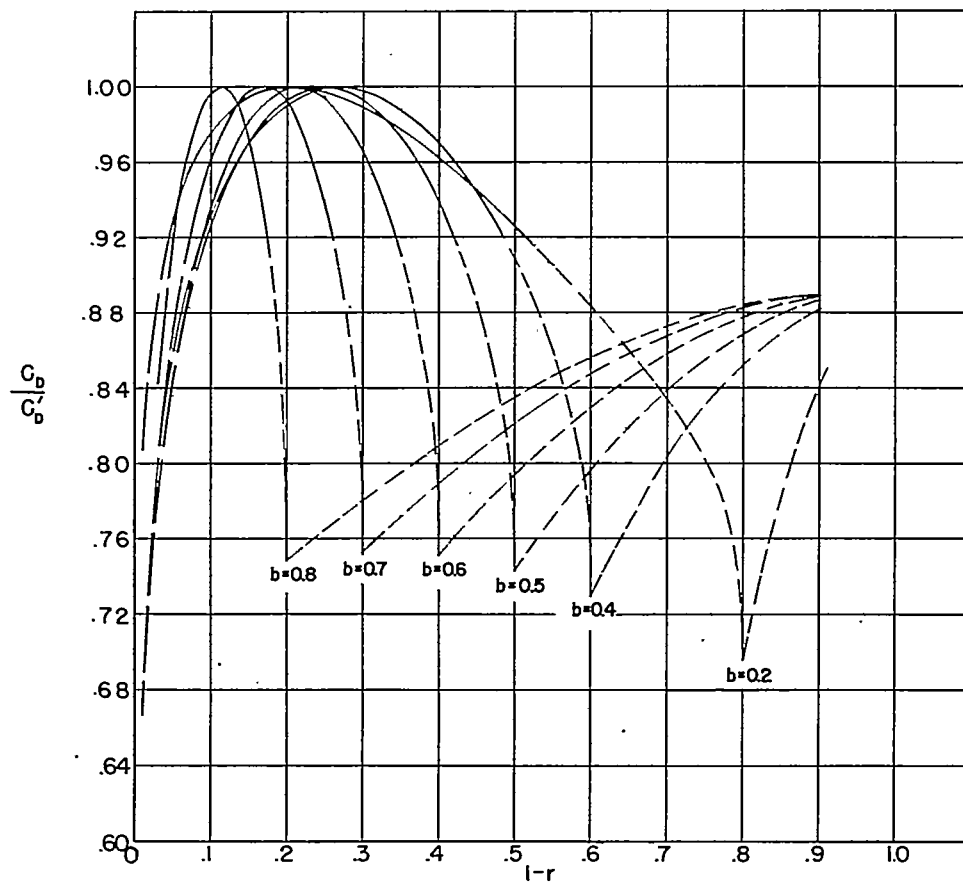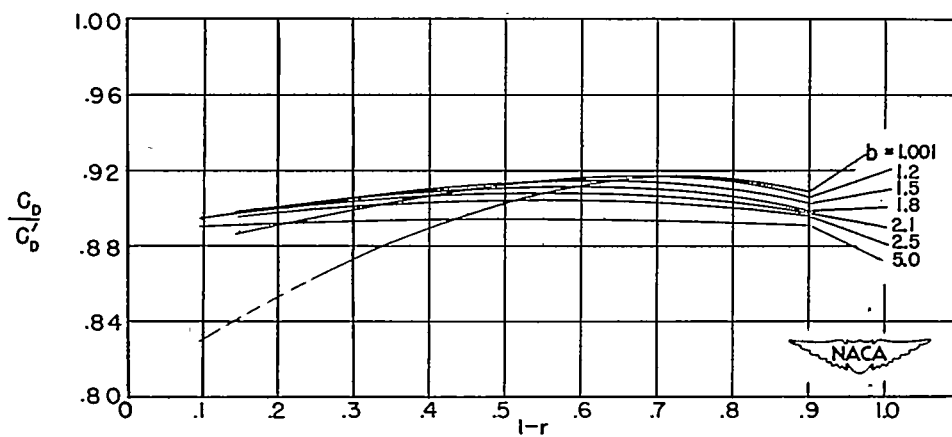volume considerations with $1 - r$ for different values of b.

(a) C_D/C_D' for G- and H-functions.

(b) C_D/C_D' for F-functions.

Figure 12.- Variation of C_D/C_D' with $1 - r$ for different values of b
using the values of $\bar{m}$ from figure 11.
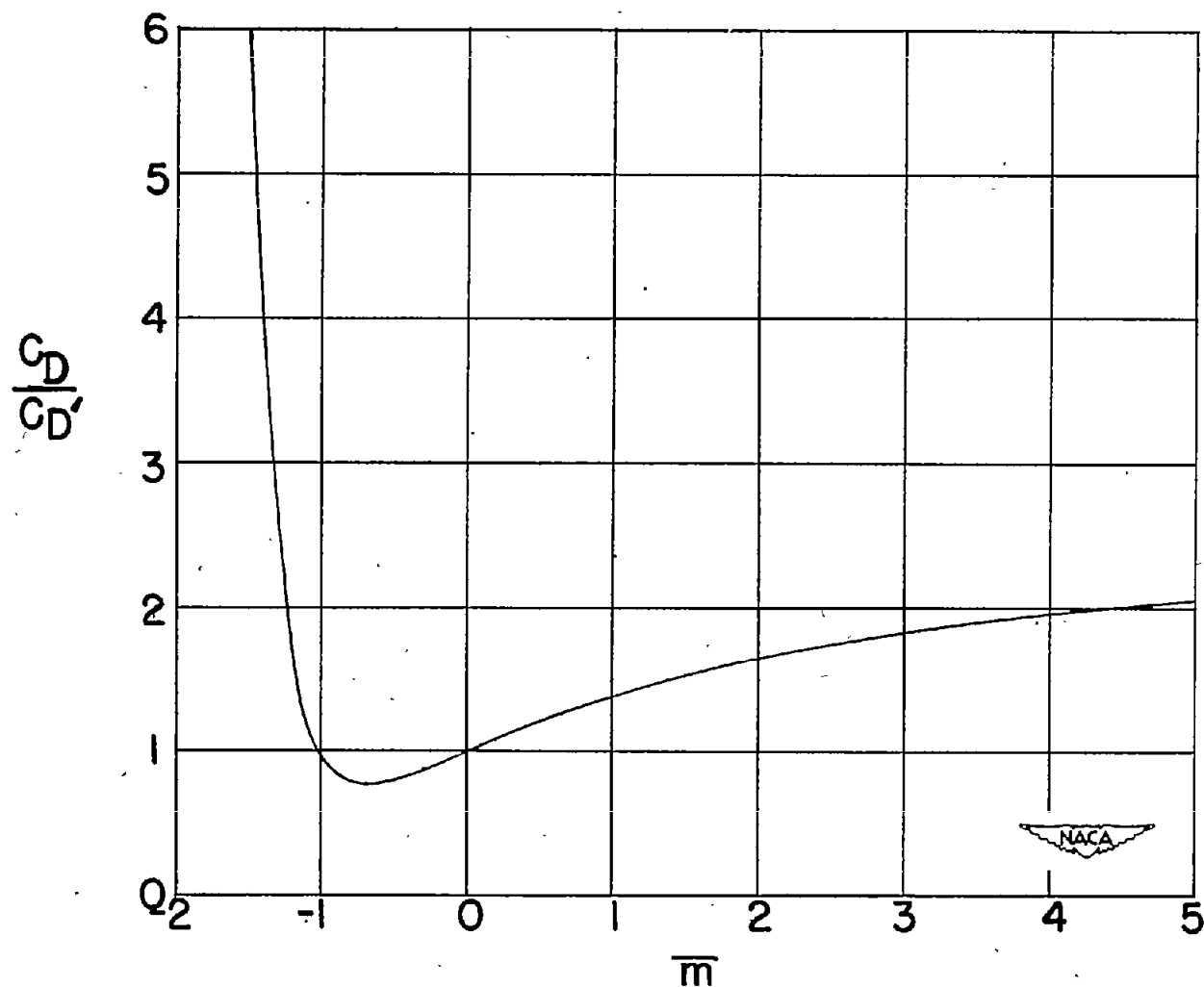
Figure 13.- Variation of C_D/C_D' with $\overline{m}$ for a case when the $\overline{m}$ for minimum C_D/C_D' prescribes a fictitious maximum thickness distribution. $b = 0.5$, $r = 0.55$.